Cell

Emerging enterococcus pore-forming toxins with MHC/HLA-I as receptors

Graphical abstract

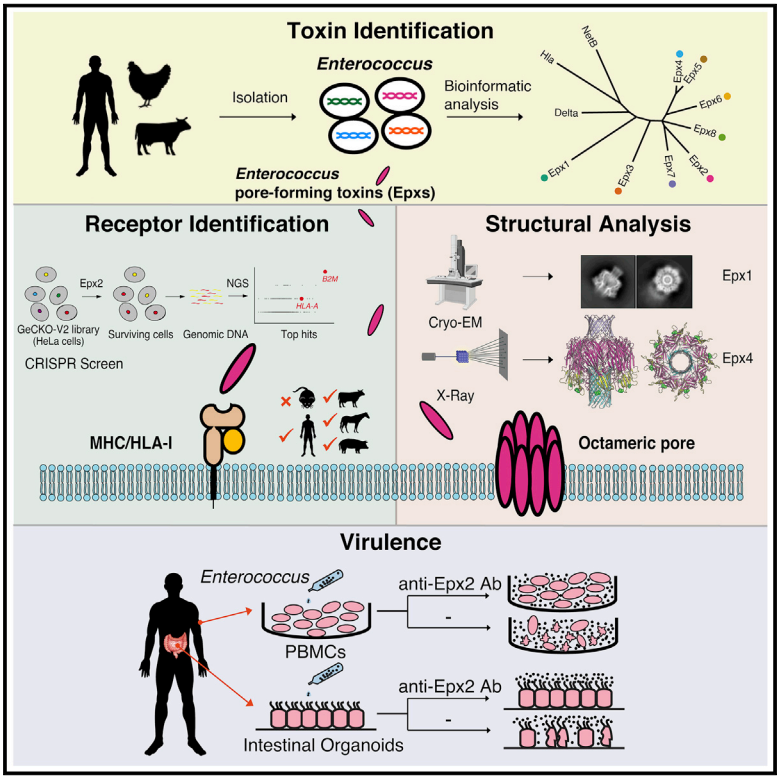

Highlights

- A family of novel pore-forming toxins (Epx1–8) is identified in genus *Enterococcus*
- Structural studies reveal a unique top domain and homo-octameric pore assembly
- CRISPR-Cas9 screen identifies MHC/HLA-I as a receptor for Epx family members
- Toxin-carrying *E. faecium* damages human PBMCs and intestinal organoids through Epx

Authors

Xiaozhe Xiong, Songhai Tian, Pan Yang, ..., Michael S. Gilmore, Jonathan Abraham, Min Dong

Correspondence

michael_gilmore@meei.harvard.edu (M.S.G.), jonathan_abraham@hms.harvard.edu (J.A.), min.dong@childrens.harvard.edu (M.D.)

In brief

Pore-forming toxins are identified in Enterococcus species isolated from nature as well as from human samples. The most potent of these toxins bind to the HLA-I in humans and MHC-I in other animals and represent an important family of canonical protein toxins in enterococci.

Xiong et al., 2022, Cell *185*, 1–15
March 31, 2022
https://doi.org/10.1016/j.cell.2022.02.002

Cell

CellPress

Article

Emerging enterococcus pore-forming toxins with MHC/HLA-I as receptors

Xiaozhe Xiong,[1,2,14] Songhai Tian,[1,2,14] Pan Yang,[2,14] Francois Lebreton,[2,3,4,5,14] Huan Bao,[6] Kuanwei Sheng,[7] Linxiang Yin,[1,2] Pengsheng Chen,[1,2] Jie Zhang,[1] Wanshu Qi,[8] Jianbin Ruan,[9,11] Hao Wu,[10] Hong Chen,[10] David T. Breault,[8,12] Hao Wu,[9] Ashlee M. Earl,[4] Michael S. Gilmore,[2,3,4,*] Jonathan Abraham,[2,4,13,*] and Min Dong[1,2,15,*]

[1]Department of Urology, Boston Children's Hospital, Department of Surgery, Harvard Medical School, Boston, MA 02115, USA
[2]Department of Microbiology, Harvard Medical School, Boston, MA 02115, USA
[3]Department of Ophthalmology, Harvard Medical School, Massachusetts Eye and Ear Infirmary, Boston, MA 02114, USA
[4]Broad Institute of MIT and Harvard, Cambridge, MA 02142, USA
[5]Multidrug-Resistant Organism Repository and Surveillance Network (MRSN), Walter Reed Army Institute of Research, Silver Spring, MD 20910, USA
[6]Department of Molecular Medicine, The Scripps Research Institute, Jupiter, FL 33458, USA
[7]Wyss Institute for Biologically Inspired Engineering, Harvard University, Boston, MA 02115
[8]Division of Endocrinology, Boston Children's Hospital, and Department of Pediatrics, Harvard Medical School, Boston, MA 02115, USA
[9]Program in Cellular and Molecular Medicine, Boston Children's Hospital, and Department of Biological Chemistry and Molecular Pharmacology, Harvard Medical School, Boston, MA 02115, USA
[10]Vascular Biology Program, Department of Surgery, Boston Children's Hospital and Harvard Medical School, Boston, MA 02115, USA
[11]Department of Immunology, University of Connecticut Health School of Medicine, Farmington, CT 06030, USA
[12]Harvard Stem Cell Institute, Cambridge, MA 02138, USA
[13]Division of Infectious Diseases, Department of Medicine, Brigham and Women's Hospital, Boston, MA 02115, USA
[14]These authors contributed equally
[15]Lead contact
*Correspondence: michael_gilmore@meei.harvard.edu (M.S.G.), jonathan_abraham@hms.harvard.edu (J.A.), min.dong@childrens.harvard.edu (M.D.)
https://doi.org/10.1016/j.cell.2022.02.002

SUMMARY

Enterococci are a part of human microbiota and a leading cause of multidrug resistant infections. Here, we identify a family of *Enterococcus* pore-forming toxins (Epxs) in *E. faecalis*, *E. faecium*, and *E. hirae* strains isolated across the globe. Structural studies reveal that Epxs form a branch of β-barrel pore-forming toxins with a β-barrel protrusion (designated the top domain) sitting atop the cap domain. Through a genome-wide CRISPR-Cas9 screen, we identify human leukocyte antigen class I (HLA-I) complex as a receptor for two members (Epx2 and Epx3), which preferentially recognize human HLA-I and homologous MHC-I of equine, bovine, and porcine, but not murine, origin. Interferon exposure, which stimulates MHC-I expression, sensitizes human cells and intestinal organoids to Epx2 and Epx3 toxicity. Co-culture with Epx2-harboring *E. faecium* damages human peripheral blood mononuclear cells and intestinal organoids, and this toxicity is neutralized by an Epx2 antibody, demonstrating the toxin-mediated virulence of Epx-carrying *Enterococcus*.

INTRODUCTION

Conversion of harmless bacteria into pathogens by mobile elements has been described since the landmark 1950s finding that diphtheria toxin was conveyed by a temperate phage (Freeman, 1951). Enterococci are a part of gut commensal bacteria of land-based animals (Lebreton et al., 2017). Since the 1970s, *Enterococcus faecalis* and *E. faecium* have emerged as leading causes of multidrug resistant (MDR) infections (Arias and Murray, 2012; Fiore et al., 2019; Gilmore et al., 2013; Lebreton et al., 2013; Van Tyne and Gilmore, 2014). Recent studies have also reported a role of *E. faecalis* in alcoholic liver disease (Duan et al., 2019) and a role of *E. hirae,* the third most abundant *Enterococcus* species in human microbiota, in regulating immune responses to tumor antigens (Fluckiger et al., 2020). Enterococci are well known for their intrinsic and recently acquired resistance to antibiotics (Van Tyne and Gilmore, 2014), leading to high mortality in infections difficult to eradicate. Some isolates of *E. faecalis* express a post-translationally modified anti-microbial peptide bacteriocin known as cytolysin, which can lyse both bacteria and eukaryotic cells and contribute to pathogenesis (Coburn et al., 2004; Van Tyne et al., 2013). However, the genus *Enterococcus* is not known to express any potent protein toxin family with an established specificity targeting human and animal cells.

Pore-forming toxins (PFTs) are the most common class of bacterial toxins (Dal Peraro and van der Goot, 2016; Los

Please cite this article in press as: Xiong et al., Emerging enterococcus pore-forming toxins with MHC/HLA-I as receptors, Cell (2022), https://doi.org/10.1016/j.cell.2022.02.002

et al., 2013). They are produced as soluble monomers that oligomerize and form transmembrane pores on cell surfaces. A variety of PFTs have evolved to disrupt epithelial barriers, disable immune cells, and damage tissues. PFTs can be divided into α-PFTs with transmembrane pores composed of α helices and β-PFTs with pores composed of β barrels. β-PFTs further include two classes of small β-barrel PFTs—the haemolysin and aerolysin families—as well as the cholesterol-dependent cytolysin family that forms large pores (Dal Peraro and van der Goot, 2016).

The well-studied *Staphylococcus aureus* α-hemolysin (Hla, also known as αHL or α-toxin) is the archetype for the haemolysin family (Berube and Bubeck Wardenburg, 2013). It is produced as a 292-residue monomer and assembles into a mushroom-shaped heptameric pore (Song et al., 1996). Other haemolysin family members include *S. aureus* leukocidin toxins, necrotic enteritis B-like toxin (NetB), beta toxin and delta toxin from *C. perfringens*, and *Vibrio cholerae* cytolysin toxin (Dal Peraro and van der Goot, 2016). Crystal structures of these toxins show highly conserved conformations in their monomeric states and assembled pores, with a variation consisting of bi-component leukocidin toxins forming hetero-octameric pores composed of four units of each component in alternating order (De and Olson, 2011; Guillet et al., 2004; Huyet et al., 2013; Olson et al., 1999; Pédelacq et al, 1999; Savva et al., 2013; Song et al., 1996; Sugawara et al., 2015; Tanaka et al., 2011; Yamashita et al., 2011, 2014; Yan et al., 2013). The archetypical aerolysin forms heptameric β-barrel transmembrane pores as well but differs from Hla in the overall domain arrangement (Degiacomi et al., 2013; Parker et al., 1994).

Although small β-barrel PFTs can form pores non-specifically at high concentrations *in vitro*, specific host protein receptors have been identified, establishing the key role of receptors in determining toxin host species and cell type selectivity (Alonzo et al., 2013; Bruggisser et al., 2020; DuMont et al., 2013; Reyes-Robles et al., 2013; Spaan et al., 2013, 2017; Tromp et al., 2018; Wilke and Bubeck Wardenburg, 2010). For instance, *S. aureus* leukocidin toxins Panton-Valentine leukocidin (PVL), γ-haemolysin CB (HlgCB), and leukocidin A/B (LukAB) recognize the human orthologs of their respective receptors, but not the murine orthologs (DuMont et al., 2013; Perelman et al., 2021; Spaan et al., 2013, 2017).

As part of ongoing surveillance studies of enterococci genomes collected from animals and the environment, we identified two uncharacterized small β-barrel PFTs homologous to haemolysin family members. Searching public databases revealed a family of β-barrel PFTs in *E. faecalis*, *E. faecium*, and *E. hirae*. Structural studies revealed that these toxins form a sub-class of the haemolysin family. Through a genome-wide CRISPR-Cas9 screen, we identified human leukocyte antigen class I (HLA-I) complex as a receptor for two of these toxins, which recognize human HLA-I and homologous major histocompatibility complex class I (MHC-I) of equine, bovine, and porcine, but not murine, origin. We further showed that a toxin-harboring *E. faecium* strain induces death of peripheral blood mononuclear cells (PBMCs) and damages intestinal organoids in a toxin-dependent manner during co-culture, demonstrating toxin-mediated virulence.

RESULTS

Toxin discovery and genome analysis

To understand how the natural reservoir of *Enterococcus* traits predisposes them to emerge as MDR hospital pathogens, we have collected and sequenced enterococcal strains since 2011. In 2018, we observed a potential small β-barrel PFT gene in an *E. faecalis* strain from chicken meat from North Carolina and another in an *E. faecium* strain from horse feces collected in Montana, which we termed *Enterococcus* pore-forming toxins 1 and 2 (Epx1 and Epx2), respectively. The closest homolog is *C. perfringens* delta toxin (42% and 43% identity to Epx1 and Epx2, respectively). Searching public databases revealed two more toxins (Epx3 and Epx4) at the beginning of our study, and our most recent search identified four additional homologs (Epxs5–8) (Goncharov et al., 2016; Manson et al., 2019; Poyet et al., 2019; Rushton-Green et al., 2019; Tyson et al., 2018; Weigand et al., 2014; Zaheer et al., 2020). These Epxs are 40%–89% identical to each other and form a separate branch from other PFTs (Figure 1A; Table S1).

Epxs have been identified in three *Enterococcus* species: Epxs1 and 3 in *E. faecalis*, Epxs2 and 7 in *E. faecium*, and Epxs4, 5, 6, and 8 in *E. hirae* (Figure 1B; Table S2). These strains were collected across five continents and from diverse sources such as chicken meat, turkey, dairy cows, horse feces, mouse colon, 40,000-year-old mammoth intestine, and wastewater, as well as human samples (stool, bodily fluid, a gluteal abscess in the United States, and a liver abscess in France) (Figure 1C; Table S2).

Comparing the genomes of these isolates with available reference genomes (WGS RefSeq) of *E. faecalis* (n = 1743; Figure 1D), *E. faecium* (n = 2197; Figure 1E), and *E. hirae* (n = 190; Figure 1F) reveals that Epx-carrying isolates are not monophyletic, indicating multiple acquisition events. Notably, an Epx1-carrying *E. faecalis* isolate, belonging to a highly persistent ST-108 lineage of poultry and human isolates, carries the vancomycin-resistance gene (Figure 1D; Table S2). Furthermore, Epx2-carrying *E. faecium* strains are closely related to known lineages of hospital-adapted MDR isolates of *E. faecium* clade A (Figure 1E) (Lebreton et al., 2013).

Further analysis of the DNA surrounding the *epx* genes revealed no overall conservation between different Epx types, except for Epxs4 and 5 within *E. hirae* (Figure S1). However, within each Epx type, the genetic organization was conserved. No common auxiliary regulatory or secretion systems were found (Figure S1). Analysis of isolates with complete genomes (n = 6) suggested that *epx1*, *2*, and *6* are conveyed by large conjugative plasmids in three strains of *E. faecalis*, *E. faecium*, and *E. hirae*, respectively, whereas *epx4*, *5*, and *8* are localized within the chromosomes of *E. hirae* strains (Figure S1).

Long-read sequencing of the Epx2-harboring *E. faecium* strain DIV0147 (isolated in the United States) confirmed that *epx2* is in a repUS15 family plasmid (named p0147_Epx2; Figure 1G). An identical Epx2 gene was found in another *E. faecium* isolate, 58M, from Siberia (Goncharov et al., 2016) that shared 98.9% nucleotide identity with DIV0147. The Epx2-carrying plasmids in 58M and DIV0147 are nearly identical (>97% nucleotide identity), suggesting that both strains vertically inherited the

Please cite this article in press as: Xiong et al., Emerging enterococcus pore-forming toxins with MHC/HLA-I as receptors, Cell (2022), https://doi.org/10.1016/j.cell.2022.02.002

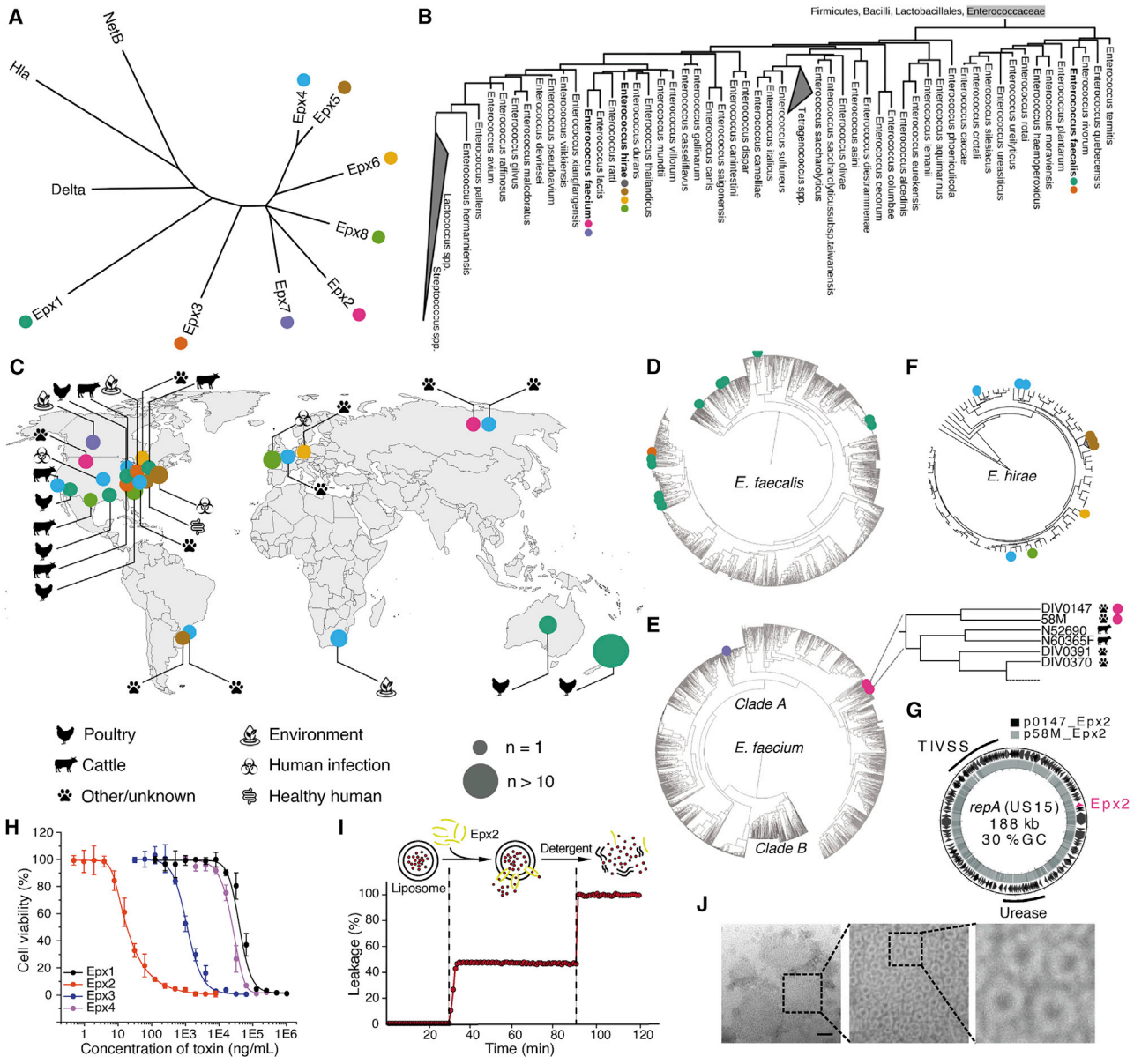

Figure 1. Identification and analysis of Epxs

(A) Maximum likelihood phylogeny of Epx toxins based on amino acid alignments. The scale bar represents the mean number of amino acid substitutions per site. Each toxin was assigned a color code. NetB, *C. perfringens* necrotic enteritis B-like toxin; Hla, *S. aureus* α-hemolysin; delta, *C. perfringens* delta toxin.

(B) 16S-based phylogeny of the *Enterococcus* genus shows that Epxs are detected in three distinct species.

(C) Global geographical distribution and source of isolation for Epx-carrying *Enterococcus* strains (marked with colored dots).

(D–F) Genome-based phylogenetic trees comparing Epx-carrying *Enterococcus* isolates with the diverse sets of publicly available (RefSeq NCBI dataset) *E. faecalis* (n = 1743) (D), *E. faecium* (n = 2197) (E), and *E. hirae* (n = 190) (F). Branch lengths reflect the number of substitutions per site.

(G) Comparison of Epx2-carrying repUS15 plasmids found in DIV0147 and 58M. TIVSS, Type IV secretion system and pilus assembly; urease, urea catabolism operon.

(H) HeLa cells were exposed to Epxs1, 2, 3, and 4 for 4 h. Cell viability was measured using MTT assays. Error bars indicate mean ± SD, N = 3.

(I) Epx2 (2 μM) induced leakage of liposomes and release of fluorescent dye sulforhodamine B. Representative curves are shown from two independent experiments.

(J) Negative staining EM of liposomes after incubation with Epx2 (2 μM), showing that Epx2 forms pores on liposomes. Scale bar, 50 nm.

See also Figures S1, S2, and S3 and Tables S1 and S2.

Please cite this article in press as: Xiong et al., Emerging enterococcus pore-forming toxins with MHC/HLA-I as receptors, Cell (2022), https://doi.org/10.1016/j.cell.2022.02.002

Epx2-plasmid. The plasmid backbone includes genes encoding a type IV secretion system and pilus assembly likely associated with its conjugative ability. These plasmids showed lower GC content (~30%) than the average *Enterococcus* chromosome (37%–38%).

Epxs are cytotoxic PFTs

To validate the function of Epxs, we produced Epxs1–4 in *E. coli* (Figures S2, S3A, and S3B). All four Epxs at a concentration of 100 μg/mL induced death of human embryonic kidney 293 (HEK293) cells (Figure S3C). We then assessed the susceptibility of a range of human cell lines (HEK293, HeLa, A549, Huh7, U2OS, and 5637; Figures 1H and S3D) and cell lines from other species (green monkey Vero cells, an immortalized mouse bone marrow-derived macrophage (BMDM) cell line, dog MDCK cells, and *Drosophila* S2 cells; Figure S3E) by exposing cells to dilutions of toxins and measuring cell viability with the MTT assay.

Epx2 is one of the most potent PFTs known for HeLa cells, with the dose resulting in loss of viability of 50% cells (IC_{50}) at ~11–14 ng/mL, which is ~100-fold more toxic than Epx3 and ~3,000-fold more toxic than Epx1 and Epx4 (Figure 1H). Epx1 and Epx4 showed IC_{50} >25 μg/mL on all cell lines (Figure S3D), whereas Epx2 and Epx3 showed variable toxicity for different cell lines (Figure S3D). Vero cells are highly sensitive to Epx2 and Epx3, whereas the toxicities on BMDM, MDCK, and S2 cells are low for all four Epxs (Figure S3E).

All four Epxs are capable of inducing lysis of artificial liposomes *in vitro* (Figures 1I and S3F). The presence of liposomes promoted formation of sodium dodecyl sulfate (SDS)-resistant oligomers similar to other PFTs (Figure S3G), and we directly observed Epx2 pores on liposomes by negative-staining electron microscopy (EM; Figure 1J).

Crystal structure of an Epx4 octameric pore

We next carried out crystallization screens and obtained the crystals of Epx4, which diffracted to 3.0 Å resolution (Figures 2A and 2B; Table S3). The structure unexpectedly revealed an assembled octameric pore instead of a monomer (Figure 2A). This is likely due to the presence of 40% 2-methyl-2,4-pentanediol (MPD) in the crystallization buffer, which has been shown to induce pore formation of Hla, γ-hemolysin, and leukocidin toxins during crystallization (Tanaka et al., 2011; Yamashita et al., 2011, 2014). The overall architecture of the Epx4 pore resembles that of Hla, comprised of a cap domain formed by the core β-sandwich region (Figures 2A and 2B), a rim domain with patches of aromatic residues that likely contact cell membranes (Figure 2C), and a stem domain forming a transmembrane β-barrel pore, with an estimated diameter of ~18 Å (Figures 2A and 2B). The cap, rim, and stem domains of the Epx4 protomer are structurally similar to the protomers of Hla (PDB: 7AHL) (Song et al., 1996), with the root mean square deviation (RMSD) at 1.415 Å (Figures 2D and 2E). However, the octameric configuration of Epx4 pore has not been reported for a single component β-barrel PFT.

An unexpected feature of the Epx4 pore is the formation of a second β barrel that sits on top of the cap region (Figures 2A–2E). We termed it the "top domain," which is formed by a β hairpin located at the N terminus of each protomer (residues 34–61; Figures 2D and S2). The diameter of this top domain is similar to that of the transmembrane β-barrel pore. The top domain, the cap region, and the stem β-barrel pore form a continuous channel, with the top domain extending the channel by 28 Å (Figures 2E and 2F).

Cryo-EM structure of Epx1 prepore

Among Epxs, we observed that Epx1 spontaneously formed SDS-resistant oligomers in solution (Figure S3G). We took advantage of this feature and conducted single particle cryogenic electron microscopy (cryo-EM) analysis of soluble Epx1 oligomers (Figures 3A and S4), which revealed assembled octameric pores, allowing us to determine a 2.9 Å structure, as well as intermediate assemblies (Figures 3A and S4C; Table S4). The overall architecture is similar to that of the Epx4 pore (Figures 3B, 3C, S5A, and S5B), with an RMSD of 0.83 Å (Figure 3D), except that the bottom third of the β-barrel pore of Epx1 was not visible in cryo-EM maps (residues 176–184; Figures 3B and 3C). This is reminiscent to the pre-pore state for γ-hemolysin and leukocidin toxins in solution (Yamashita et al., 2014), in which a pore-like configuration is assembled but the last third of the β barrel remains disordered (Figure S5C).

To further confirm that Epx1 forms functional pores, we analyzed the conductance properties of Epx1 on planar lipid bilayers through single-channel electrophysiological recordings. Multiple stepwise pore-forming events were observed (Figures S3H–S3J). The conductance of the pore varied linearly with the applied potential and did not show rectification (Figure S3K). The conductance (290 ± 20 pS) in combination with the estimated length of the pore based on our structure suggests a pore diameter of ~2.1 ± 0.1 nm.

The top domain is crucial for toxicity

The structures of Epx1 and Epx4 revealed extensive inter-protomer interactions mediated by charged residues within their top domains (Figure 3E). Mutations at two charged residues (K50E and K50E/K54E in Epx1 and K51E and K51E/K57E in Epx4) in the top domain, which does not alter the overall conformation of Epx proteins measured by circular dichroism spectroscopy (Figure S5D), reduced the efficacy of forming SDS-resistant oligomers (Figure S5E) and toxicity on HeLa cells (Figure 3F). Similarly, mutating analogous residues (K50E and K50E/K56E) in Epx2 disrupted formation of SDS-resistant oligomers (Figures S5D and S5E) and abolished toxicity on HeLa cells (Figure 3F).

Structure-based sequence alignments suggest that the top domain of Epxs corresponds to the N-terminal latch domain (Figure S2), which has been suggested to play a role in inter-protomer interactions (Huyet et al., 2013; Sugawara et al., 2015), in other Hla family members. Epx members share a conserved overall length and number of charged residues within this region, whereas Hla has a large gap within this region, missing 14 of the 30 residues (Figure S2).

CRISPR-Cas9 screen identifies MHC/HLA-I as a receptor for Epx2

We next focused on identification of cellular receptors for Epx2 using genome-wide CRISPR-Cas9 screens, as this toxin showed different toxicity levels across a range of cell lines (Figure S3D). A genome-wide single-guide RNA (sgRNA) library (GeCKO-v2) was transduced in HeLa cells that stably express

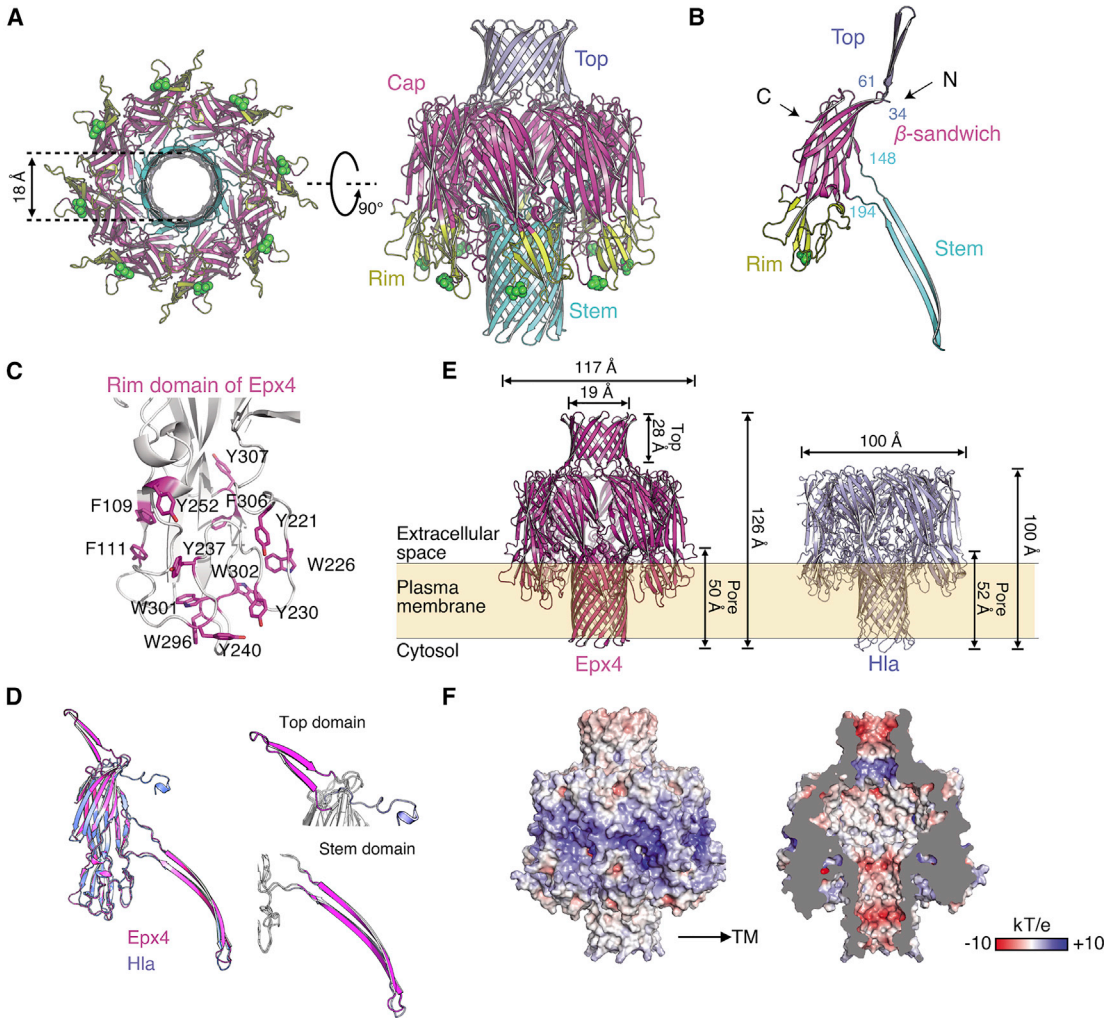

Figure 2. Crystal structure of Epx4 octameric pore

(A) Bottom and side view of a ribbon diagram of the 3.0 Å crystal structure of the Epx4 pore. The top, cap, rim, and stem domains are colored in light blue, magenta, yellow, and cyan, respectively. MPD molecules bound to Epx4 are shown as green spheres.

(B) The structure of the Epx4 protomer. The top, β sandwich, rim, and stem domains are colored in light blue, magenta, yellow, and cyan, respectively. The N terminus (N), C terminus (C), and residue numbers for the top domain and the stem domain are marked.

(C) Ribbon diagram of the rim domain of Epx4. The side chains of exposed aromatic residues are shown as sticks and labeled.

(D) Superimposition of the Epx4 (magenta) and Hla (light blue; PDB: 7AHL) protomers (Song et al., 1996). The N-terminal top region and the stem domain are enlarged in the right panels.

(E) Comparison of the size and configuration of the Epx4 pore versus the Hla pore (PDB: 7AHL).

(F) Electrostatic surface representation of the Epx4 pore. Viewed from the membrane side (left) and the pore interior side (right). Electrostatic potential is expressed as a spectrum ranging from −10 kT/e (red) to +10 kT/e (blue). TM, transmembrane.

See also Table S3.

Cas9 (Figure S6A) (Sanjana et al., 2014; Tao et al., 2016; Tian et al., 2018). Cells were selected with increasing concentrations of Epx2 (Figure 4A). The top hit is β-2-microglobulin (*B2M*) (Figures 4B and S6B). Other hits included sorting nexin-17 (*SNX17*) and G antigen 1 (*GAGE1*) (Figure 4B).

B2M is a small protein (119 residues) that serves as the β chain of MHC-I (Bjorkman et al., 1987; Neefjes et al., 2011; Pamer and Cresswell, 1998; Wieczorek et al., 2017). B2M binds to a polymorphic α-chain protein to form MHC/HLA-I complexes (Figure 4C). There are three major α-chain genes (*HLA-A*, *-B*, *and -C*) and three minor α-chain genes (*HLA-E*, *-F*, *and -G*) in humans (Neefjes et al., 2011; Wieczorek et al., 2017). HLA-A was also identified in our screen (Figure 4B). All of these α chains, which are composed of a single transmembrane domain with an extracellular region divided into three domains (α1–3), need to form a heterodimer with B2M (Figure 4C). Binding of B2M is critical for proper trafficking of MHC/HLA-I onto cell surfaces; thus, a lack of B2M would block cell surface expression of all MHC/HLA-I complexes.

To validate the top hits, we generated stable knockout (KO) HeLa cells lacking B2M, HLA-A, SNX17, or GAGE1. B2M KO

Please cite this article in press as: Xiong et al., Emerging enterococcus pore-forming toxins with MHC/HLA-I as receptors, Cell (2022), https://doi.org/10.1016/j.cell.2022.02.002

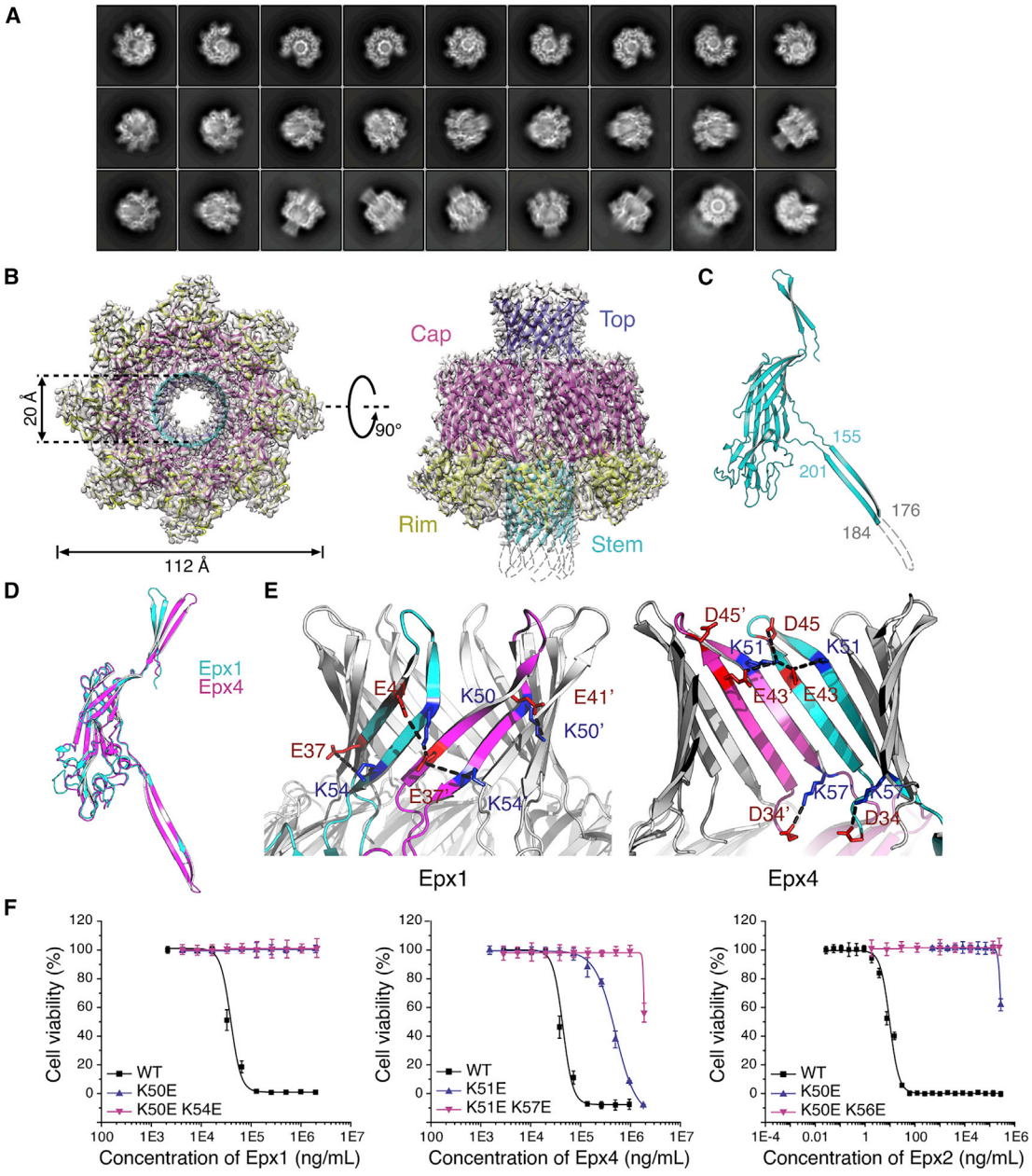

Figure 3. Cryo-EM structure of Epx1 prepore

(A) 2D class averages of Epx1 particles.

(B) Cryo-EM map (gray, 2.9 Å resolution) superimposed onto the atomic model of the octameric Epx1 prepore. Density was not observed for residues 176 to 184, and these are shown as dashed lines. The top, cap, rim, and stem domains are colored in light blue, magenta, yellow, and cyan respectively.

(C) The structure of Epx1 protomer. The regions that were not resolved are shown as dashed lines.

(D) The structure of the Epx1 protomer (cyan) and its superimposition with the Epx4 protomer (magenta).

(E) The top domains of Epx1 (left panel) and Epx4 (right panel) are enlarged to indicate crucial polar interactions (dashed lines).

(F) Mutations that disrupt polar interactions in the top domains of Epx1 (K50E and K50E/K54E), Epx4 (K51E and K51E/K57E), and Epx2 (K50E and K50E/K56E) abolished cytotoxicity on HeLa cells. Error bars indicate mean ± SD, N = 3.

See also Figures S2, S3, S4, and S5 and Table S4.

cells showed over 13,000-fold reduction in sensitivity to Epx2 compared with wild-type (WT) HeLa cells (Figures 4D and 4E). HLA-A KO cells showed ~14-fold reduced sensitivity to Epx2 (Figure 4E). SNX17 and GAGE1 showed slight reduction in sensitivity but did not reach statistical significance (Figure S6C). In addition, B2M KO cells also became resistant to Epx3, whereas their sensitivity to Epxs1 and 4 was not changed (Figures 4F and S6D–S6F).

Please cite this article in press as: Xiong et al., Emerging enterococcus pore-forming toxins with MHC/HLA-I as receptors, Cell (2022), https://doi.org/10.1016/j.cell.2022.02.002

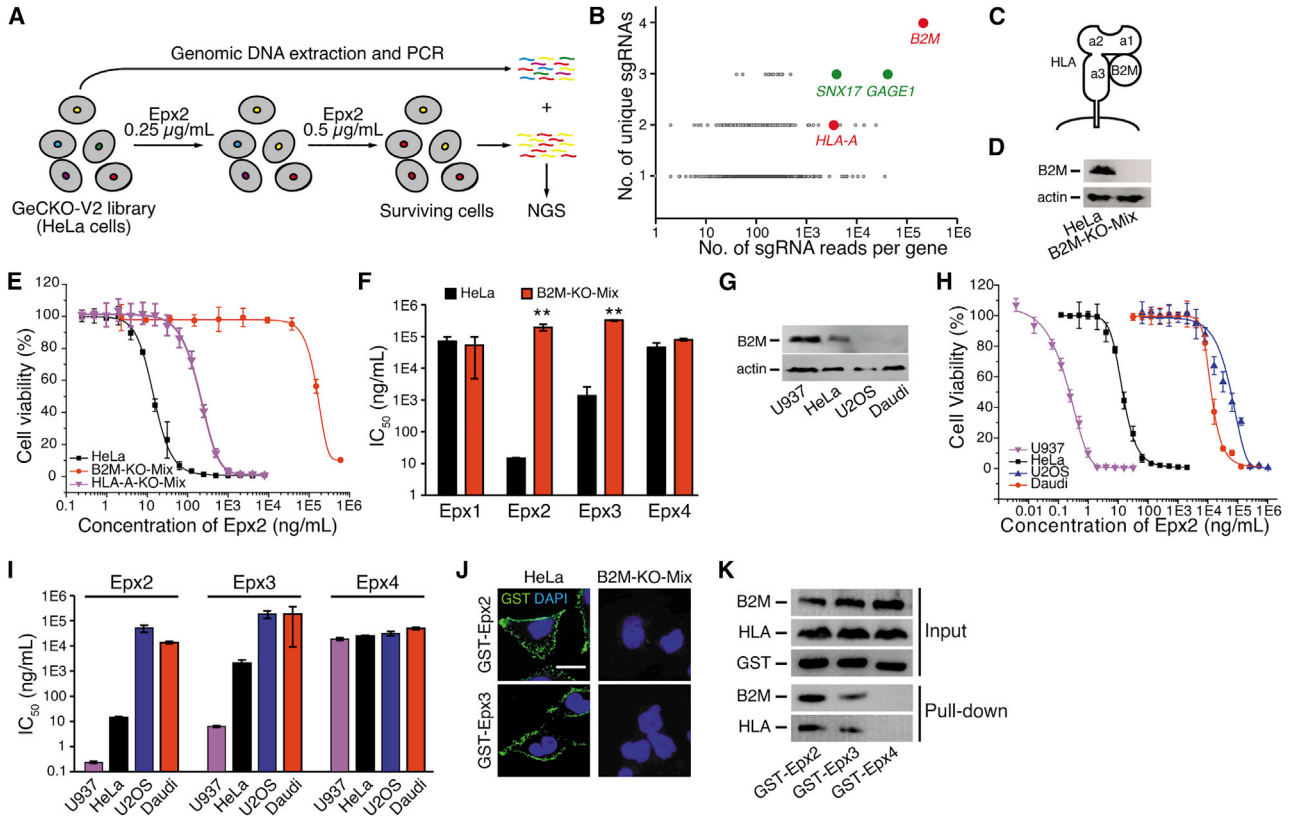

Figure 4. Genome-wide CRISPR/Cas9 screen identifies MHC/HLA-I as a receptor for Epx2

(A) Schematic diagram of the screening process. NGS, next-generation sequencing.

(B) Genes identified from the screen were plotted based on the number of unique sgRNAs (y axis) and total sgRNA reads (x axis).

(C) Schematic drawing of the HLA-I complex.

(D) Immunoblot analysis of cell lysates showed that B2M expression was abolished in mixed stable B2M knockout (KO) HeLa cells. Actin served as a loading control.

(E and F) Mixed stable B2M KO and HLA-A KO HeLa cells showed reduced sensitivity to Epx2 compared with wild-type (WT) HeLa cells (E). The IC_{50} values were plotted in (F). Error bars indicate mean ± SD, N = 3. **p < 0.01.

(G) Cell lysates of four human cell lines (U937, HeLa, U2OS, and Daudi) were analyzed by immunoblot to detect their endogenous B2M levels. Actin served as the loading control.

(H and I) The sensitivity of U937, HeLa, U2OS, and Daudi cells to Epx2 was analyzed using MTT assays (H). The IC_{50} values were plotted in (I). Error bars indicate mean ± SD, N = 3.

(J) Immunostaining analysis showed that GST-tagged Epx2 and Epx3 bound to WT HeLa cells, but not B2M KO cells. GST-Epx2 and -Epx3 were detected using anti-GST antibody. Nuclei were labeled with DAPI. Scale bar, 5 μm.

(K) Immunoblot analysis showed that GST tagged Epx2 and Epx3, but not Epx4, pulled down endogenous HLA-A and B2M from HeLa cell lysates.

(D, G, J, and K) Representative images were from one of three independent experiments.

See also Figure S6.

We also tested three human cancer cell lines, with two (U2OS and Daudi cells) that did not express detectable levels of B2M and one (U937 cells) that has B2M levels higher than HeLa cells (Figure 4G). U937 showed an IC_{50} value of 0.2 ng/mL for Epx2 and 6 ng/mL for Epx3, ~70- to 200-fold more sensitive than HeLa cells, whereas U2OS and Daudi cells had IC_{50} values of over 13 μg/mL with Epxs2, 3, and 4 (Figures 4H, 4I, and S6K).

We generated Epxs2 and 3 proteins fused with a glutathione *S*-transferase (GST) tag at their N-termini. By detecting the GST tag, we found that GST-Epx2 and -Epx3 did not bind to B2M KO cells (Figures 4J and S6L). Furthermore, endogenous B2M and HLA-A in HeLa cell lysates could be pulled down by GST-Epx2 and -Epx3, while GST-Epx4 showed no binding (Figure 4K).

Epx2 and Epx3 recognize HLA/MHC-I complex

To determine whether toxins recognize B2M alone, HLA alone, or the heterodimer complex, we expressed B2M, B2M fused with an antigen peptide, HLA-A, B2M fused with HLA-A, and B2M plus a peptide fused with HLA-A in HEK293 cells (Figure 5A). GST-Epx2 and -Epx3 pulled down HLA complexes, with or without the fused peptide, but not B2M alone or HLA-A alone from cell lysates (Figure 5B). GST-Epx2 and -Epx3 pulled down B2M-HLA-B and B2M-HLA-C complexes as well, but not HLA-B or HLA-C alone (Figure 5C). Consistent with these

Please cite this article in press as: Xiong et al., Emerging enterococcus pore-forming toxins with MHC/HLA-I as receptors, Cell (2022), https://doi.org/10.1016/j.cell.2022.02.002

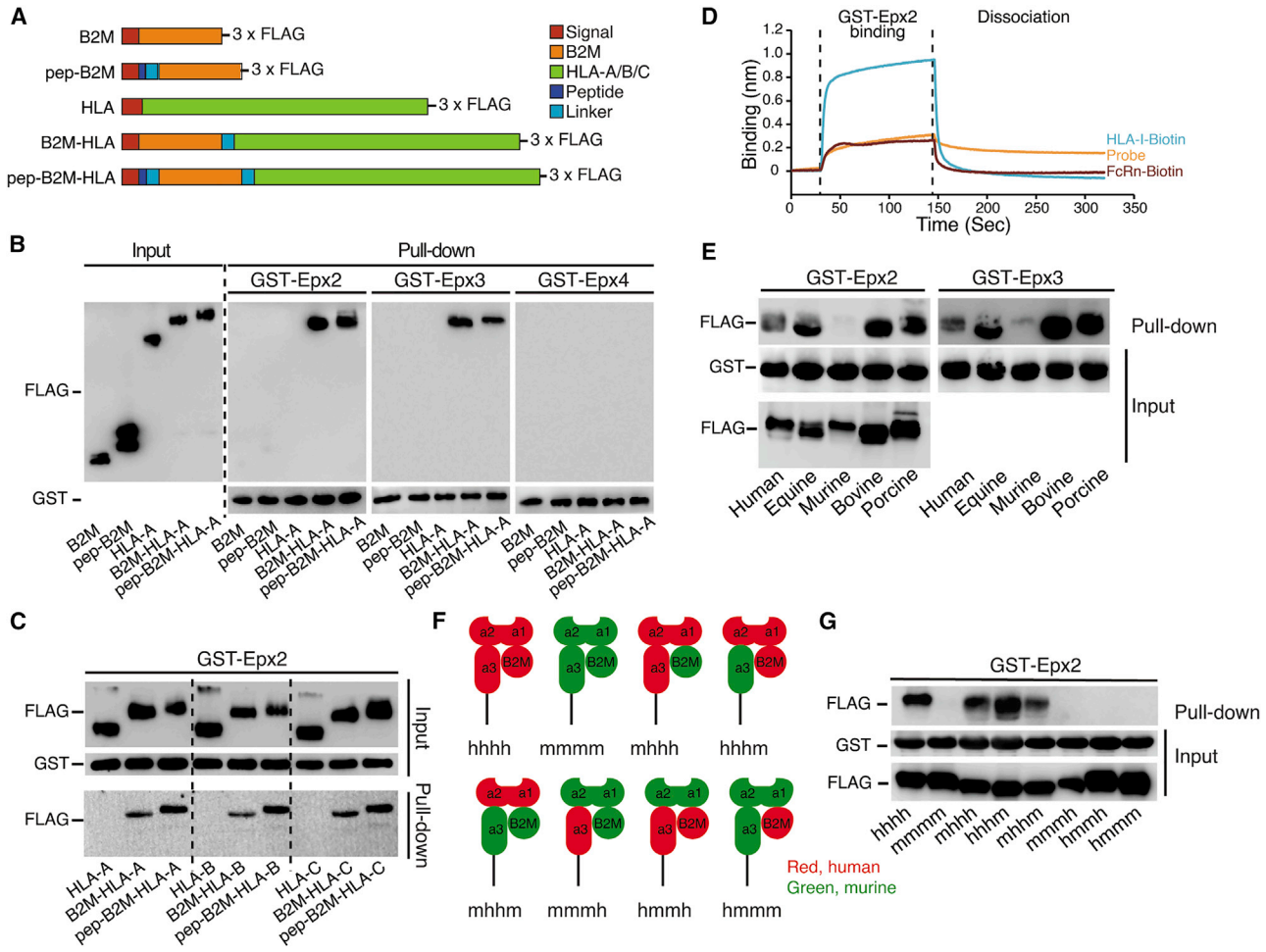

Figure 5. Epx2 and 3 recognize HLA/MHC-I complexes

(A) Schematic diagram of B2M, B2M fused with a peptide (pep-B2M), HLA-A, B2M fused with HLA-A, and a fusion protein containing a peptide, B2M, and HLA-A. All are tagged with 3× FLAG at their C termini.

(B) HEK293 cells were transfected with the above constructs, and cell lysates were subjected to pull-down assays using GST-tagged Epx2, Epx3, and Epx4. B2M-HLA fusion proteins (B2M-HLA and pep-B2M-HLA), but not B2M alone (B2M and pep-B2M) or HLA-A alone, can be pulled down by GST-Epx2 and -Epx3.

(C) FLAG-tagged HLA-A, HLA-B, HLA-C, and their fusion proteins with B2M or B2M plus a peptide (pep-B2M) were expressed in HEK293 cells. Pull-down experiments with GST-Epx2 were carried out.

(D) Direct binding of GST-Epx2 to biotin-labeled HLA-I complex was characterized using biolayer interferometry. Neonatal Fc receptor (FcRn) and empty probe were analyzed as controls.

(E) FLAG-tagged human, murine, equine, bovine, and porcine versions of MHC-I α-subunit fused with their own B2M were expressed in HEK293 cells. Cell lysates were collected and split into two equal parts for pull-down assays using GST-tagged Epx2 and Epx3, respectively.

(F and G) Six chimeric FLAG-tagged MHC-I complexes were generated by switching α1-α2, α3, or B2M between human (red) and murine (green) versions (F). These chimeric MHC-I complexes were expressed in HEK293 cells, and pull-down assays were carried out with GST-Epx2 (G).

(B, C, E, and G) Representative images were from one of three independent experiments.

See also Figure S7.

results, GST-Epx2 did not interact with purified B2M in pull-down assays (Figure S7A).

We next assayed for direct binding of GST-Epx2 to biotinylated HLA-I complex using biolayer interferometry (Figure 5D). GST-Epx2 did not bind to biotinylated neonatal Fc receptor complex (FcRn), despite FcRn containing B2M as a subunit (Figure 5D) (Simister and Mostov, 1989). The binding affinity between GST-Epx2 and HLA-I complex is weak, with a K_D (dissociation constant) in the micromolar range (Figures S7B and S7C). It is possible that a proper membrane environment and multi-valent interactions are required for high-affinity binding of Epx2 on cell surfaces.

Epx2 had low activity on murine cells (Figure S3E). Human and murine B2M and α-subunit share ~86% and ~65% sequence identity, respectively. To assess the potential species selectivity, human, murine, equine, bovine, and porcine versions of MHC-I α-subunit fused with their own B2M were expressed in HEK293 cells (Figure 5E). GST-tagged Epx2 and Epx3 pulled

Please cite this article in press as: Xiong et al., Emerging enterococcus pore-forming toxins with MHC/HLA-I as receptors, Cell (2022), https://doi.org/10.1016/j.cell.2022.02.002

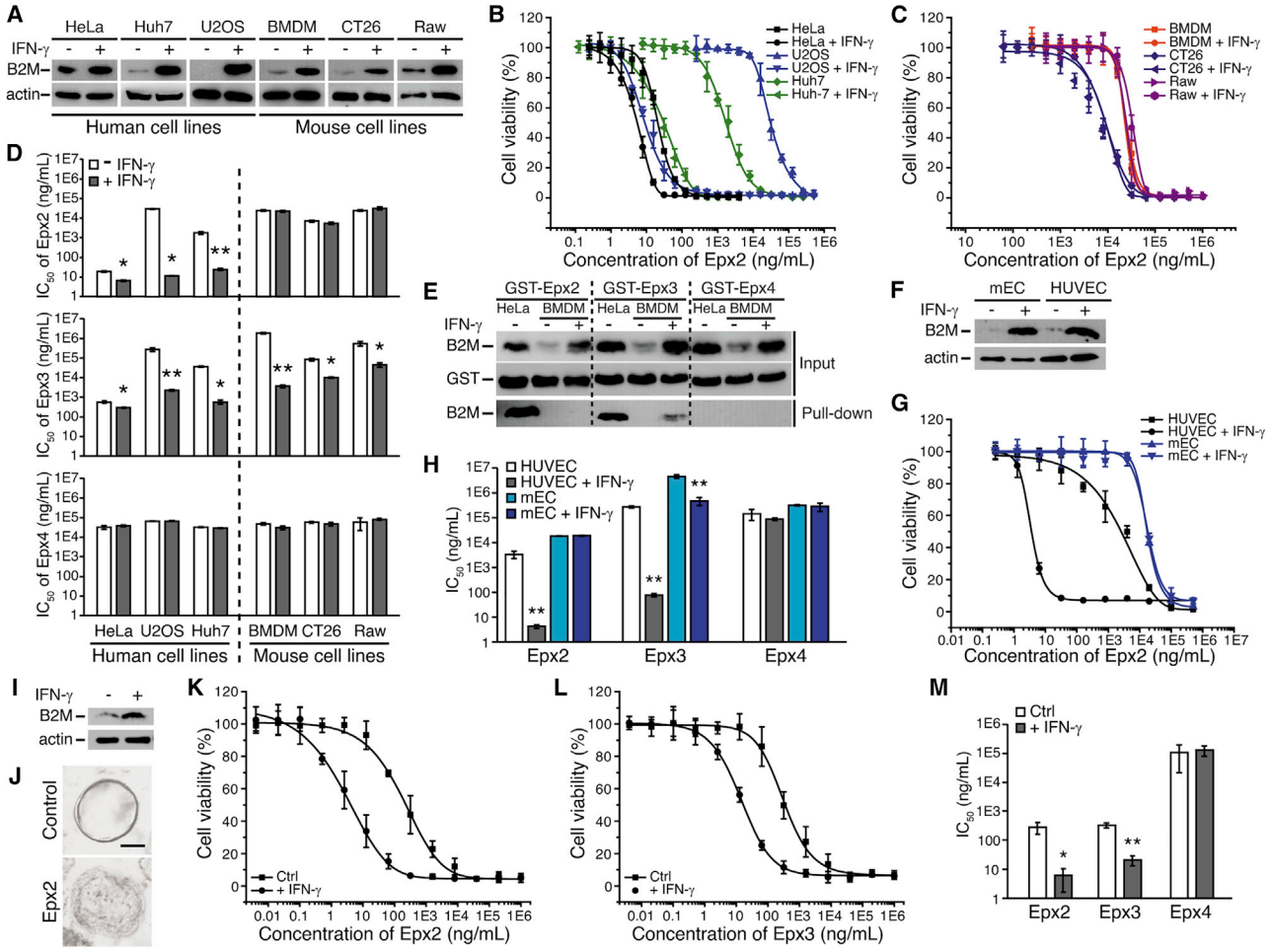

Figure 6. IFN-γ sensitizes human cells and intestinal organoids to Epx2 and Epx3

(A) IFN-γ treatment elevated MHC-I complex levels in human and mouse cell lines, as demonstrated by immunoblot analysis of B2M in cell lysates. Actin served as a loading control.

(B–D) IFN-γ treatment increased sensitivity of human cell lines (HeLa, U2OS, and Huh7) to Epx2 (B) but did not change the sensitivity of mouse cell lines (BMDM, CT26, and Raw) (C). IC_{50} values for Epx2, Epx3, and Epx4 are summarized in (D). Error bars indicate mean ± SD, N = 3. *p < 0.05; **p < 0.01 (Student's t test).

(E) Immunoblot analysis showed that GST-Epx2 did not pull down mouse B2M from BMDM lysates, whereas GST-Epx3 weakly pulled down B2M from BMDM lysates upon treatment with IFN-γ.

(F) IFN-γ treatment increased MHC-I levels in primary cultured mouse endothelial cells (mECs) and human umbilical vein endothelial cells (HUVECs). Actin served as a loading control.

(G and H) IFN-γ treatment increased sensitivity of HUVECs, but not mECs, to Epx2 (G). IC_{50} values for Epx2, Exp3, and Epx4 on HUVECs and mECs with and without IFN-γ treatment are summarized in (H). Error bars indicate mean ± SD, N = 3. **p < 0.01 (Student's t test).

(I) IFN-γ treatment increased B2M levels in cultured human intestinal organoids.

(J) Representative images showing that Epx2 (100 ng/mL, 30 min incubation) induced death of cultured human intestinal organoids. Scale bar, 100 μm.

(K–M) Human intestinal organoids are sensitive to both Epx2 (K) and Epx3 (L), and their sensitivities are further increased after IFN-γ treatment. These organoids are not sensitive to Epx4 and IFN-γ treatment did not alter the sensitivity to Epx4 (M). Ctrl, control. *p < 0.05; **p < 0.01 (Student's t test).

(A, E, F, I, and J) Representative images were from one of two independent experiments.

See also Figure S7.

down human, equine, bovine, and porcine MHC-I, but not murine MHC-I (Figure 5E).

To further map the toxin binding site, we swapped domains between mouse MHC-I and HLA-I. The α1 and α2 domains of the HLA α-subunit form the peptide presentation site, and the α3 domain is next to the transmembrane domain (Figure 5F). We switched α1-α2, α3, and B2M between human and mouse versions (Figure 5F). Pull-down assays indicated that B2M does not contain the toxin binding site. Instead, the binding site for Epx2 is located on the α1-α2 region of the HLA/MHC-I α-subunit (Figure 5G).

IFN-γ sensitizes human cells and intestinal organoids to Epx2 and Epx3

Expression of HLA/MHC-I is known to be greatly elevated by interferons (primarily IFN-γ, but also by IFN-α and -β) as part of the

Please cite this article in press as: Xiong et al., Emerging enterococcus pore-forming toxins with MHC/HLA-I as receptors, Cell (2022), https://doi.org/10.1016/j.cell.2022.02.002

immune response to viral and bacterial pathogens (Fellous et al., 1982; Gough et al., 2012). We thus compared the sensitivity of three human cell lines (HeLa, Huh7, and U2OS) and three murine cell lines (BMDM, CT26, and Raw) to Epxs with and without pretreatment of IFN-γ. As expected, HLA/MHC-I levels were elevated after exposure to IFN-γ (Figure 6A). This increase rendered Huh7 cells ~70-fold and U2OS cells >2700-fold more sensitive to Epx2 and Huh7 cells 61-fold and U2OS cells ~118-fold more sensitive to Epx3 (Figures 6B, 6D, S7D, and S7E). The sensitivity of HeLa cells was also increased to Epx2 and Epx3 after exposure to IFN-γ (Figures 6B and 6D). The sensitivities of these cells to Epx4 remain unchanged (Figures 6D, S7F, and S7G). Three murine cell lines showed no changes in their sensitivity to Epx2 and Epx4 but had increased sensitivity to Epx3 after IFN-γ treatment (Figures 6C, 6D, S7E, and S7G). Consistent with these results, GST-Epx2 was able to pull down B2M from HeLa cells, but not from BMDM (Figure 6E), whereas Epx3 was still able to weakly pull down murine MHC-I (Figure 6E).

To characterize the toxicity of Epx2 and Epx3 on primary cells, we first tested primary human umbilical vein endothelial cells (HUVECs) and mouse lung endothelial cells (mECs). IFN-γ treatment increased B2M levels in HUVECs and mECs (Figure 6F). After IFN-γ treatment, the IC_{50} value of Epx2 with HUVECs decreased from 3.2 μg/mL to 4.2 ng/mL (819 fold), and the IC_{50} value of Epx3 with HUVECs decreased from 268 μg/mL to 75 ng/mL (>3,500 fold) (Figures 6G, 6H, and S7H). Epx2 showed no change in toxicity on mECs after IFN-γ treatment (Figures 6G and 6H). mECs showed an increase in sensitivity to Epx3 after IFN-γ treatment, although the overall level of sensitivity remained low (Figure S7H). The sensitivities of HUVECs and mECs to Epx4 were not changed after IFN-γ treatment (Figures 6H and S7I).

We next examined human intestinal organoids (Figure 6I). Intestinal organoids were sensitive to Epx2 and Epx3 even without IFN-γ treatment (IC_{50} of 277 ng/mL for Epx2 and 323 ng/mL for Epx3; Figures 6J–6M), and exposure to IFN-γ further enhanced their sensitivity (6 ng/mL for Epx2 and 21 ng/mL for Epx3) (Figure 6M). Human organoids were not sensitive to Epx4 (IC_{50} at 104 μg/mL) with or without IFN-γ treatment (Figures 6M and S7J).

Native Epx2 produced by *E. faecium* DIV0147 is toxic to human cells

To investigate whether Epx toxins produced by *Enterococcus* contribute to virulence for human cells, we focused on the Epx2-carrying *E. faecium* strain DIV0147 as a representative. A closely related strain, DIV0391, which shares ~98.9% DNA sequence identity with DIV0147 but does not have an *epx2* gene, was utilized as a control. Furthermore, we produced a rabbit polyclonal antibody against Epx2, which can neutralize Epx2 toxicity on HeLa cells (Figure 7A). It did not cross react with Epxs1, 3, or 4 and had no effect on Epx3 toxicity on HeLa cells (Figures S7K and S7L).

Mass spectrometry analysis detected Epx2 directly in the supernatant of DIV0147 (Figure S7M). The concentrated supernatant of DIV0147 induced death of HeLa cells, whereas the supernatant of the control DIV0391 strain showed no toxicity. The toxicity of DIV0147 supernatant was neutralized by the Epx2 antibody (Figure 7B). We note that we had to concentrate the supernatant in order to detect toxins, indicating that toxin production is suppressed under lab culture conditions.

We then investigated co-culture of *E. faecium* bacteria with human cell lines (HeLa and U937 cells). Co-culture with DIV0147 for 6 h resulted in death of all cells, whereas cell viability was not affected by co-culture with the control strain (Figures 7C and 7D). Adding the Epx2 antibody into the medium eliminated toxicity (Figures 7C and 7D). Furthermore, DIV0147 showed no toxicity when co-cultured with B2M KO HeLa cells (Figure 7E). These results demonstrate that Epx2 is solely responsible for the toxicity exhibited by DIV0147 on human cell lines.

E. faecium DIV0147 uses Epx2 to damage human PBMCs and intestinal organoids

Immune suppression is a major function of many PFTs. Indeed, co-culture with DIV0147 damaged freshly isolated human PBMCs as measured by a lactate dehydrogenase (LDH) release assay, whereas the control strain showed no toxicity (Figure 7F). Adding a polyclonal Epx2 antibody neutralized the toxicity of DIV0147.

Disruption of epithelial barriers is another common function of PFTs. We cultured human intestinal organoids as monolayers in *trans*-wells (Figure 7G). We then carried out co-culture experiments by adding *E. faecium* into the upper compartment of the *trans*-well. Co-culture with DIV0147 for 8 h damaged intestinal organoid monolayers as measured by LDH release assays and disrupted cell-cell junctions as detected by increased leakage of a dextran-conjugated dye from the upper compartment into the lower compartment of the *trans*-well (Figure 7G). The control strain had no toxicity, and adding Epx2 antibody eliminated DIV0147 toxicity completely (Figure 7G).

DISCUSSION

Traits that exacerbate human infection often evolve and emerge from natural reservoirs outside of humans and historically were often not recognized until they spread into human populations. The genomic era now provides us with a powerful way to identify new potential threats to human health. With their highly malleable genomes (Paulsen et al., 2003), enterococci can serve as a hub for inter-species gene transfer, such as the transmission of vancomycin resistance to methicillin-resistant strains of *S. aureus* (Weigel et al., 2003). Unlike many other Gram-positive pathogens in the genera *Streptococcus*, *Staphylococcus*, and *Clostridium*, toxins targeting human and animal cells are rare in enterococci. We previously identified a botulinum neurotoxin-like toxin in a single *E. faecium* strain, but the targeted host species remains unknown for this toxin (Zhang et al., 2018). Here, we identified and characterized a family of β-barrel PFTs in enterococci, with members highly toxic to human cells. The widespread geographical distribution, the diversity of hosts, and the clear evidence for multiple independent introductions into distinct species all suggest that acquisition of this family of toxins is not a rare event and likely confers competitive advantages.

Our functional characterizations reveal the pathogenic potential of toxin-harboring *E. faecium* and suggest a key role of Epx2 in immune suppression and epithelial barrier disruption during

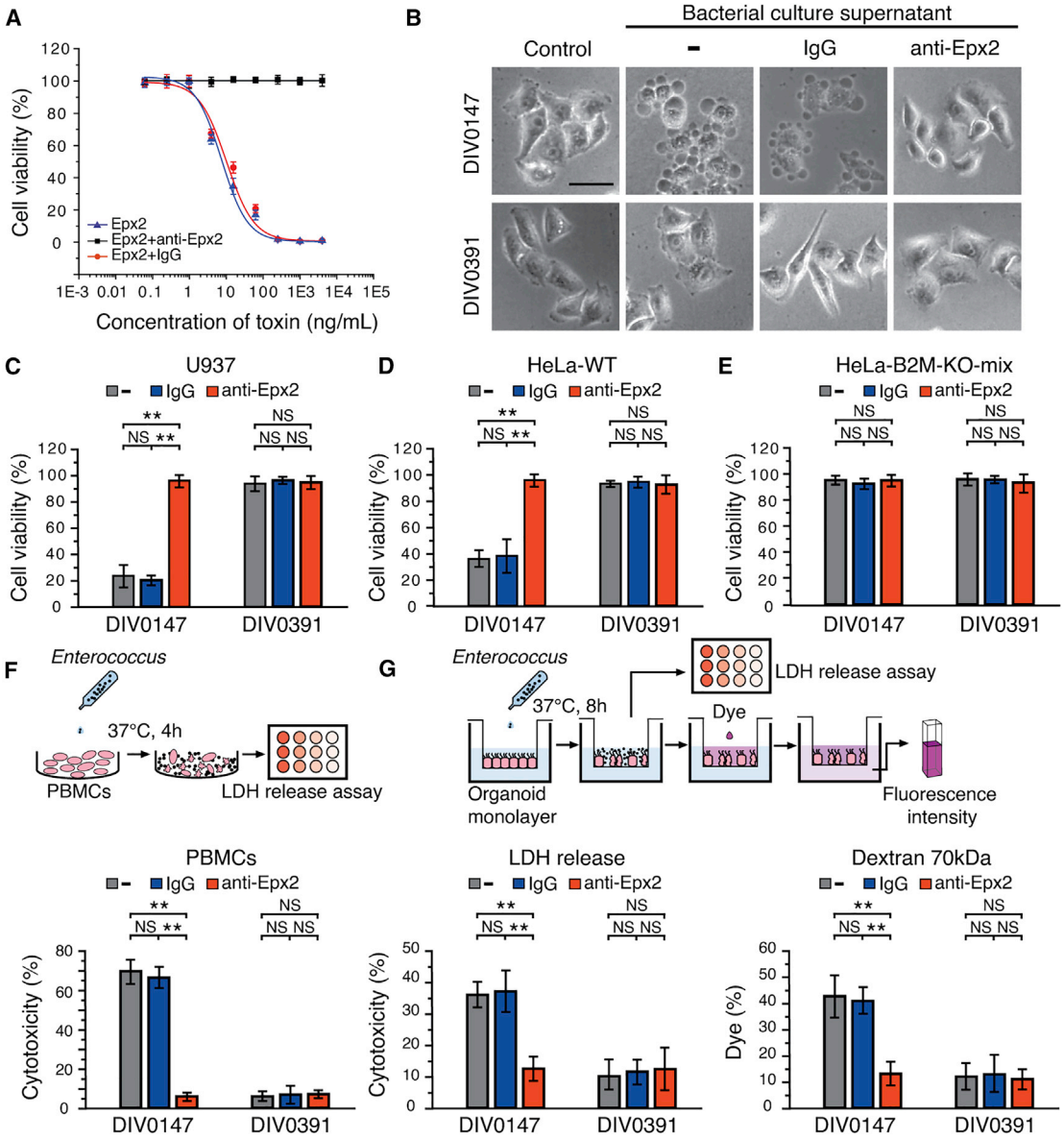

Figure 7. Co-culture with *E. faecium* DIV0147 damages human PBMCs and intestinal organoids through Epx2

(A) A rabbit polyclonal antibody against Epx2 neutralized the toxicity of Epx2 toxin on HeLa cells. Immunoglobin G (IgG) served as a control.

(B) *E. faecium* DIV0147 culture supernatant induced death of HeLa cells, and this toxicity was neutralized by an Epx2 antibody. The supernatant from a control strain that lacks *epx2* gene, *E. faecium* DIV0391, did not show any toxicity to cells. Scale bar, 50 μm.

(C and D) Co-culture with *E. faecium* DIV0147 (MOI = 800, 6 h) resulted in death of U937 (C) and HeLa cells (D). This toxicity is neutralized by an Epx2 antibody. Co-culture with a control strain *E. faecium* DIV0391 did not show any toxicity to cells.

(E) Co-culture with *E. faecium* DIV0147 did not affect the viability of B2M KO HeLa cells.

(F) Co-culture with *E. faecium* DIV0147 (MOI = 800, 4 h) damaged human PBMCs measured by LDH release assays. This toxicity was neutralized by an Epx2 antibody. Co-culture with a control strain *E. faecium* DIV0391 did not show any toxicity to cells.

(G) Human intestinal organoids were cultured as monolayers on trans-wells. *E. faecium* DIV0147 was added to the upper compartment during co-culture (MOI = 800, 8 h), which damaged intestinal organoids (detected by LDH release assays) and increased the dye leakage into the lower chamber. This toxicity is neutralized by an Epx2 antibody.

(C–G) **$p < 0.01$, not significant (NS), $p > 0.05$ (Student's t test).

See also Figure S7.

pathogenesis. Besides humans, Epx2 and Epx3 can also recognize the MHC-I of major agricultural animals including horses, cattle, and pigs, which may serve as natural reservoirs for enterococci harboring these potent toxins. Considering that MDR hospital-adapted *E. faecium* strains co-evolved with animal populations as they spread into humans (Lebreton et al., 2013),

expansion of Epxs into strains of hospital-adapted lineages has the potential to be a devastating development.

By switching domains between human HLA-I and murine MHC-I, we were able to map the binding site for Epx2 to α1-α2 domains of MHC-I, which are the polymorphic domains containing the peptide binding site for antigen presentation and the region engaging the T cell receptor. Binding appears to be mediated by conserved regions on α1-α2, since Epx2 can bind to all three HLA-A, HLA-B, and HLA-C forms. Interestingly, superantigens, another class of bacterial toxins such as *S. aureus* toxic shock syndrome toxin 1 recognize the polymorphic α1 domain of MHC-II (Jardetzky et al., 1994; Karp et al., 1990; Kim et al., 1994), which is also the domain containing the peptide binding site and engaging the T cell receptor. Determining the structure of an Epx2-MHC-I complex will be required to elucidate the mechanism of toxin-receptor recognition.

MHC-I is expressed on all nucleated cells, but not on red blood cells. It presents peptide antigens derived from cytosolic proteins degraded by proteasomes. Recognition of foreign or mutated peptide antigens by $CD8^+$ T cells then induces cell death to eliminate infected or cancerous cells (Neefjes et al., 2011; Wieczorek et al., 2017). The level of MHC-I is greatly increased by interferons under inflammatory conditions. IFN-γ plays a critical role in regulating both innate and adaptive host responses to not only viral infections but also to a variety of bacterial pathogens such as *S. aureus*, *Salmonella typhimurium*, *Listeria monocytogenes*, and *Mycobacterium tuberculosis* (Shtrichman and Samuel, 2001). Interestingly, commensal microbes such as *Bacteroidetes* induce and maintain a low level of IFN-β production from colonic dendritic cells (Abt et al., 2012; Stefan et al., 2020), which primes intestinal tissues in a vigilant state against potential viral infections. Finally, Epx2 and Epx3 are potential tools to induce death of virally infected cells and cancerous cells in humans in an IFN-dependent manner.

Limitations of the study

The pathogenic potential of Epx-harboring bacteria and the role of Epxs remain to be investigated and validated *in vivo* in animal infection models. A major technical limitation is that mice and rats are not suitable models, as Epx2 does not recognize murine MHC-I. Whether Epxs and the bacteria that produce them cause, or will cause, any human or animal diseases remains a major question to be investigated. Epx1 and Epx4 did not show high levels of toxicity on cell lines we have tested. This is likely because these cells do not have their receptors. We cannot exclude the possibility that Epxs assembled as active pores on cell membranes could differ from the structures of Epx1 and Epx4 we obtained in solution in this study, and future studies resolving the pore structure in lipid membranes will be important.

STAR★METHODS

Detailed methods are provided in the online version of this paper and include the following:

SUPPLEMENTAL INFORMATION

Supplemental information can be found online at https://doi.org/10.1016/j.cell.2022.02.002.

ACKNOWLEDGMENTS

We thank members of Dong lab for discussions and Dr. Xiangdong Zheng for helping with structure refinement. This study was partially supported by grants from National Institutes of Health (NIH) (R01NS080833, R01NS117626, R01AI132387, R01AI139087, R01AI158503, and R21NS106159 to M.D.), Director's New Innovator Award (DP2GM140920 to H.B.), Harvard-wide Program on antibiotic resistance (NIH AI083214 to M.S.G.), HHSN272200900018C and U19AI110818 to A.M.E., and Intelligence Advanced Research Projects Activity (IARPA) (W911NF-17-2-0089 to M.D.). This work is based upon research conducted at the Northeastern Collaborative Access Team (NE-CAT) beamlines (P30 GM124165). The Pilatus 6M detector on 24-ID-C beam line is funded by a NIH-ORIP HEI grant (S10 RR029205). This research used resources of the Advanced Photon Source: a U.S. Department of Energy (DOE) Office of Science User Facility operated by Argonne National Laboratory under contract No. DE-AC02-06CH11357. M.D. and D.T.B. acknowledge support from the NIH-funded Harvard Digestive Disease Center (P30DK034854), and M.D. acknowledges support from the Boston Children's Hospital Intellectual and

Developmental Disabilities Research Center (P30HD18655). M.D. holds the Investigator in the Pathogenesis of Infectious Disease award from the Burroughs Wellcome Fund. J.A. is a recipient of a Career Award for Medical Scientists from the Burroughs Wellcome Fund.

AUTHOR CONTRIBUTIONS

F.L., X.X., and M.D. conceived the project. X.X. and S.T. carried out the majority of the experiments. M.S.G. created and curated the enterococcal diversity collection. M.S.G. and A.M.E. established the EnteroGenome program. F.L. performed the bioinformatic analysis. X.X., P.Y., J.R., H.W., and J.A. carried out structure determination. H.B. carried out single-channel analysis. K.S. analyzed CRISPR-Cas9 screening data. L.Y. assisted with liposome leakage assay. J.Z. helped with generation of Epx2 antibody. P.C. carried out mass spectrum analysis. W.Q. and D.T.B. provided human organoids. H.W. (Vascular Biology Program, Boston Children's Hospital) and H.C. prepared HUVEC and mEC cells and helped with experiments on these models. F.L., X.X., S.T., and M.D. wrote the manuscript with input from all co-authors.

DECLARATION OF INTERESTS

H.W. is on the advisory board of *Cell*. Boston Children's Hospital has filed a provisional patent application on applications of Epxs described here, with X.X, S.T., and M.D. as co-inventors. The other authors declare no competing interests.

Received: July 2, 2021
Revised: December 15, 2021
Accepted: February 1, 2022
Published: March 7, 2022

REFERENCES

Abt, M.C., Osborne, L.C., Monticelli, L.A., Doering, T.A., Alenghat, T., Sonnenberg, G.F., Paley, M.A., Antenus, M., Williams, K.L., Erikson, J., et al. (2012). Commensal bacteria calibrate the activation threshold of innate antiviral immunity. Immunity *37*, 158–170.

Adams, P.D., Afonine, P.V., Bunkóczi, G., Chen, V.B., Davis, I.W., Echols, N., Headd, J.J., Hung, L.W., Kapral, G.J., Grosse-Kunstleve, R.W., et al. (2010). PHENIX: a comprehensive Python-based system for macromolecular structure solution. Acta Crystallogr. D Biol. Crystallogr. *66*, 213–221.

Alonzo, F., 3rd, Kozhaya, L., Rawlings, S.A., Reyes-Robles, T., DuMont, A.L., Myszka, D.G., Landau, N.R., Unutmaz, D., and Torres, V.J. (2013). CCR5 is a receptor for Staphylococcus aureus leukotoxin ED. Nature *493*, 51–55.

Arias, C.A., and Murray, B.E. (2012). The rise of the Enterococcus: beyond vancomycin resistance. Nat. Rev. Microbiol. *10*, 266–278.

Berube, B.J., and Bubeck Wardenburg, J. (2013). Staphylococcus aureus α-toxin: nearly a century of intrigue. Toxins (Basel) *5*, 1140–1166.

Bjorkman, P.J., Saper, M.A., Samraoui, B., Bennett, W.S., Strominger, J.L., and Wiley, D.C. (1987). Structure of the human class I histocompatibility antigen, HLA-A2. Nature *329*, 506–512.

Bruggisser, J., Tarek, B., Wyder, M., Muller, P., von Ballmoos, C., Witz, G., Enzmann, G., Deutsch, U., Engelhardt, B., and Posthaus, H. (2020). CD31 (PECAM-1) Serves as the Endothelial Cell-Specific Receptor of Clostridium perfringens beta-Toxin. Cell Host Microbe *28*, 69–78.e6.

Coburn, P.S., Pillar, C.M., Jett, B.D., Haas, W., and Gilmore, M.S. (2004). Enterococcus faecalis senses target cells and in response expresses cytolysin. Science *306*, 2270–2272.

Dal Peraro, M., and van der Goot, F.G. (2016). Pore-forming toxins: ancient, but never really out of fashion. Nat. Rev. Microbiol. *14*, 77–92.

De, S., and Olson, R. (2011). Crystal structure of the Vibrio cholerae cytolysin heptamer reveals common features among disparate pore-forming toxins. Proc. Natl. Acad. Sci. USA *108*, 7385–7390.

Degiacomi, M.T., Iacovache, I., Pernot, L., Chami, M., Kudryashev, M., Stahlberg, H., van der Goot, F.G., and Dal Peraro, M. (2013). Molecular assembly of the aerolysin pore reveals a swirling membrane-insertion mechanism. Nat. Chem. Biol. *9*, 623–629.

Duan, Y., Llorente, C., Lang, S., Brandl, K., Chu, H., Jiang, L., White, R.C., Clarke, T.H., Nguyen, K., Torralba, M., et al. (2019). Bacteriophage targeting of gut bacterium attenuates alcoholic liver disease. Nature *575*, 505–511.

DuMont, A.L., Yoong, P., Day, C.J., Alonzo, F., 3rd, McDonald, W.H., Jennings, M.P., and Torres, V.J. (2013). Staphylococcus aureus LukAB cytotoxin kills human neutrophils by targeting the CD11b subunit of the integrin Mac-1. Proc. Natl. Acad. Sci. USA *110*, 10794–10799.

Emsley, P., Lohkamp, B., Scott, W.G., and Cowtan, K. (2010). Features and development of Coot. Acta Crystallogr. D Biol. Crystallogr. *66*, 486–501.

Fellous, M., Nir, U., Wallach, D., Merlin, G., Rubinstein, M., and Revel, M. (1982). Interferon-dependent induction of mRNA for the major histocompatibility antigens in human fibroblasts and lymphoblastoid cells. Proc. Natl. Acad. Sci. USA *79*, 3082–3086.

Fiore, E., Van Tyne, D., and Gilmore, M.S. (2019). Pathogenicity of Enterococci. Microbiol. Spectr. *7*, https://doi.org/10.1128/microbiolspec.GPP3-0053-2018.

Fluckiger, A., Daillère, R., Sassi, M., Sixt, B.S., Liu, P., Loos, F., Richard, C., Rabu, C., Alou, M.T., Goubet, A.G., et al. (2020). Cross-reactivity between tumor MHC class I-restricted antigens and an enterococcal bacteriophage. Science *369*, 936–942.

Freeman, V.J. (1951). Studies on the virulence of bacteriophage-infected strains of Corynebacterium diphtheriae. J. Bacteriol. *61*, 675–688.

Gilmore, M.S., Lebreton, F., and van Schaik, W. (2013). Genomic transition of enterococci from gut commensals to leading causes of multidrug-resistant hospital infection in the antibiotic era. Curr. Opin. Microbiol. *16*, 10–16.

Goncharov, A., Grigorjev, S., Karaseva, A., Kolodzhieva, V., Azarov, D., Akhremenko, Y., Tarasova, L., Tikhonov, A., Masharskiy, A., Zueva, L., and Suvorov, A. (2016). Draft Genome Sequence of Enterococcus faecium Strain 58m, Isolated from Intestinal Tract Content of a Woolly Mammoth, Mammuthus primigenius. Genome Announc. *4*, e01706–e01715.

Gough, D.J., Messina, N.L., Clarke, C.J., Johnstone, R.W., and Levy, D.E. (2012). Constitutive type I interferon modulates homeostatic balance through tonic signaling. Immunity *36*, 166–174.

Guillet, V., Roblin, P., Werner, S., Coraiola, M., Menestrina, G., Monteil, H., Prévost, G., and Mourey, L. (2004). Crystal structure of leucotoxin S component: new insight into the Staphylococcal beta-barrel pore-forming toxins. J. Biol. Chem. *279*, 41028–41037.

Huyet, J., Naylor, C.E., Savva, C.G., Gibert, M., Popoff, M.R., and Basak, A.K. (2013). Structural Insights into Clostridium perfringens Delta Toxin Pore Formation. PLoS ONE *8*, e66673.

Jardetzky, T.S., Brown, J.H., Gorga, J.C., Stern, L.J., Urban, R.G., Chi, Y.I., Stauffacher, C., Strominger, J.L., and Wiley, D.C. (1994). Three-dimensional structure of a human class II histocompatibility molecule complexed with superantigen. Nature *368*, 711–718.

Karp, D.R., Teletski, C.L., Scholl, P., Geha, R., and Long, E.O. (1990). The alpha 1 domain of the HLA-DR molecule is essential for high-affinity binding of the toxic shock syndrome toxin-1. Nature *346*, 474–476.

Kelley, L.A., Mezulis, S., Yates, C.M., Wass, M.N., and Sternberg, M.J. (2015). The Phyre2 web portal for protein modeling, prediction and analysis. Nat. Protoc. *10*, 845–858.

Kim, J., Urban, R.G., Strominger, J.L., and Wiley, D.C. (1994). Toxic shock syndrome toxin-1 complexed with a class II major histocompatibility molecule HLA-DR1. Science *266*, 1870–1874.

Kucukelbir, A., Sigworth, F.J., and Tagare, H.D. (2014). Quantifying the local resolution of cryo-EM density maps. Nat. Methods *11*, 63–65.

Lebreton, F., van Schaik, W., McGuire, A.M., Godfrey, P., Griggs, A., Mazumdar, V., Corander, J., Cheng, L., Saif, S., Young, S., et al. (2013). Emergence of epidemic multidrug-resistant Enterococcus faecium from animal and commensal strains. MBio *4*, e00534–e00513.

Lebreton, F., Manson, A.L., Saavedra, J.T., Straub, T.J., Earl, A.M., and Gilmore, M.S. (2017). Tracing the Enterococci from Paleozoic Origins to the Hospital. Cell *169*, 849–861.e13.

Letunic, I., and Bork, P. (2016). Interactive tree of life (iTOL) v3: an online tool for the display and annotation of phylogenetic and other trees. Nucleic Acids Res. *44*, W242–245.

Los, F.C., Randis, T.M., Aroian, R.V., and Ratner, A.J. (2013). Role of pore-forming toxins in bacterial infectious diseases. Microbiol. Mol. Biol. Rev. *77*, 173–207.

Manson, A.L., Van Tyne, D., Straub, T.J., Clock, S., Crupain, M., Rangan, U., Gilmore, M.S., and Earl, A.M. (2019). Chicken Meat-Associated Enterococci: Influence of Agricultural Antibiotic Use and Connection to the Clinic. Appl. Environ. Microbiol. *85*, e01559–e01519.

Naville, M., Ghuillot-Gaudeffroy, A., Marchais, A., and Gautheret, D. (2011). ARNold: a web tool for the prediction of Rho-independent transcription terminators. RNA Biol. *8*, 11–13.

Neefjes, J., Jongsma, M.L., Paul, P., and Bakke, O. (2011). Towards a systems understanding of MHC class I and MHC class II antigen presentation. Nat. Rev. Immunol. *11*, 823–836.

Olson, R., Nariya, H., Yokota, K., Kamio, Y., and Gouaux, E. (1999). Crystal structure of staphylococcal LukF delineates conformational changes accompanying formation of a transmembrane channel. Nat. Struct. Biol. *6*, 134–140.

Otwinowski, Z., and Minor, W. (1997). Processing of X-ray diffraction data collected in oscillation mode. Methods Enzymol. *276*, 307–326.

Pamer, E., and Cresswell, P. (1998). Mechanisms of MHC class I–restricted antigen processing. Annu. Rev. Immunol. *16*, 323–358.

Parker, M.W., Buckley, J.T., Postma, J.P., Tucker, A.D., Leonard, K., Pattus, F., and Tsernoglou, D. (1994). Structure of the Aeromonas toxin proaerolysin in its water-soluble and membrane-channel states. Nature *367*, 292–295.

Paulsen, I.T., Banerjei, L., Myers, G.S., Nelson, K.E., Seshadri, R., Read, T.D., Fouts, D.E., Eisen, J.A., Gill, S.R., Heidelberg, J.F., et al. (2003). Role of mobile DNA in the evolution of vancomycin-resistant Enterococcus faecalis. Science *299*, 2071–2074.

Pédelacq, J.D., Maveyraud, L., Prévost, G., Baba-Moussa, L., González, A., Courcelle, E., Shepard, W., Monteil, H., Samama, J.P., and Mourey, L. (1999). The structure of a Staphylococcus aureus leucocidin component (LukF-PV) reveals the fold of the water-soluble species of a family of transmembrane pore-forming toxins. Structure *7*, 277–287.

Perelman, S.S., James, D.B.A., Boguslawski, K.M., Nelson, C.W., Ilmain, J.K., Zwack, E.E., Prescott, R.A., Mohamed, A., Tam, K., Chan, R., et al. (2021). Genetic variation of staphylococcal LukAB toxin determines receptor tropism. Nat. Microbiol. *6*, 731–745.

Pettersen, E.F., Goddard, T.D., Huang, C.C., Couch, G.S., Greenblatt, D.M., Meng, E.C., and Ferrin, T.E. (2004). UCSF Chimera–a visualization system for exploratory research and analysis. J. Comput. Chem. *25*, 1605–1612.

Poyet, M., Groussin, M., Gibbons, S.M., Avila-Pacheco, J., Jiang, X., Kearney, S.M., Perrotta, A.R., Berdy, B., Zhao, S., Lieberman, T.D., et al. (2019). A library of human gut bacterial isolates paired with longitudinal multiomics data enables mechanistic microbiome research. Nat. Med. *25*, 1442–1452.

Reyes-Robles, T., Alonzo, F., 3rd, Kozhaya, L., Lacy, D.B., Unutmaz, D., and Torres, V.J. (2013). Staphylococcus aureus leukotoxin ED targets the chemokine receptors CXCR1 and CXCR2 to kill leukocytes and promote infection. Cell Host Microbe *14*, 453–459.

Rushton-Green, R., Darnell, R.L., Taiaroa, G., Carter, G.P., Cook, G.M., and Morgan, X.C. (2019). Agricultural Origins of a Highly Persistent Lineage of Vancomycin-Resistant *Enterococcus faecalis* in New Zealand. Appl. Environ. Microbiol. *85*, e00137–e00119.

Sanchez-Garcia, R., Gomez-Blanco, J., Cuervo, A., Carazo, J.M., Sorzano, C.O.S., and Vargas, J. (2021). DeepEMhancer: a deep learning solution for cryo-EM volume post-processing. Commun. Biol. *4*, 874.

Sanjana, N.E., Shalem, O., and Zhang, F. (2014). Improved vectors and genome-wide libraries for CRISPR screening. Nat. Methods *11*, 783–784.

Savva, C.G., Fernandes da Costa, S.P., Bokori-Brown, M., Naylor, C.E., Cole, A.R., Moss, D.S., Titball, R.W., and Basak, A.K. (2013). Molecular architecture and functional analysis of NetB, a pore-forming toxin from Clostridium perfringens. J. Biol. Chem. *288*, 3512–3522.

Shtrichman, R., and Samuel, C.E. (2001). The role of gamma interferon in antimicrobial immunity. Curr. Opin. Microbiol. *4*, 251–259.

Simister, N.E., and Mostov, K.E. (1989). An Fc receptor structurally related to MHC class I antigens. Nature *337*, 184–187.

Song, L., Hobaugh, M.R., Shustak, C., Cheley, S., Bayley, H., and Gouaux, J.E. (1996). Structure of staphylococcal alpha-hemolysin, a heptameric transmembrane pore. Science *274*, 1859–1866.

Spaan, A.N., Henry, T., van Rooijen, W.J.M., Perret, M., Badiou, C., Aerts, P.C., Kemmink, J., de Haas, C.J.C., van Kessel, K.P.M., Vandenesch, F., et al. (2013). The staphylococcal toxin Panton-Valentine Leukocidin targets human C5a receptors. Cell Host Microbe *13*, 584–594.

Spaan, A.N., van Strijp, J.A.G., and Torres, V.J. (2017). Leukocidins: staphylococcal bi-component pore-forming toxins find their receptors. Nat. Rev. Microbiol. *15*, 435–447.

Stefan, K.L., Kim, M.V., Iwasaki, A., and Kasper, D.L. (2020). Commensal Microbiota Modulation of Natural Resistance to Virus Infection. Cell *183*, 1312–1324.e10.

Stothard, P., Grant, J.R., and Van Domselaar, G. (2019). Visualizing and comparing circular genomes using the CGView family of tools. Brief. Bioinform. *20*, 1576–1582.

Sugawara, T., Yamashita, D., Kato, K., Peng, Z., Ueda, J., Kaneko, J., Kamio, Y., Tanaka, Y., and Yao, M. (2015). Structural basis for pore-forming mechanism of staphylococcal α-hemolysin. Toxicon *108*, 226–231.

Tanaka, Y., Hirano, N., Kaneko, J., Kamio, Y., Yao, M., and Tanaka, I. (2011). 2-Methyl-2,4-pentanediol induces spontaneous assembly of staphylococcal α-hemolysin into heptameric pore structure. Protein Sci. *20*, 448–456.

Tao, L., Zhang, J., Meraner, P., Tovaglieri, A., Wu, X., Gerhard, R., Zhang, X., Stallcup, W.B., Miao, J., He, X., et al. (2016). Frizzled proteins are colonic epithelial receptors for C. difficile toxin B. Nature *538*, 350–355.

Tian, S., Muneeruddin, K., Choi, M.Y., Tao, L., Bhuiyan, R.H., Ohmi, Y., Furukawa, K., Furukawa, K., Boland, S., Shaffer, S.A., et al. (2018). Genome-wide CRISPR screens for Shiga toxins and ricin reveal Golgi proteins critical for glycosylation. PLoS Biol. *16*, e2006951.

Tromp, A.T., Van Gent, M., Abrial, P., Martin, A., Jansen, J.P., De Haas, C.J.C., Van Kessel, K.P.M., Bardoel, B.W., Kruse, E., Bourdonnay, E., et al. (2018). Human CD45 is an F-component-specific receptor for the staphylococcal toxin Panton-Valentine leukocidin. Nat. Microbiol. *3*, 708–717.

Tyson, G.H., Sabo, J.L., Hoffmann, M., Hsu, C.H., Mukherjee, S., Hernandez, J., Tillman, G., Wasilenko, J.L., Haro, J., Simmons, M., et al. (2018). Novel linezolid resistance plasmids in Enterococcus from food animals in the USA. J. Antimicrob. Chemother. *73*, 3254–3258.

Vagin, A., and Teplyakov, A. (2010). Molecular replacement with MOLREP. Acta Crystallogr. D Biol. Crystallogr. *66*, 22–25.

Van Tyne, D., and Gilmore, M.S. (2014). Friend turned foe: evolution of enterococcal virulence and antibiotic resistance. Annu. Rev. Microbiol. *68*, 337–356.

Van Tyne, D., Martin, M.J., and Gilmore, M.S. (2013). Structure, function, and biology of the Enterococcus faecalis cytolysin. Toxins (Basel) *5*, 895–911.

Wagner, T., Merino, F., Stabrin, M., Moriya, T., Antoni, C., Apelbaum, A., Hagel, P., Sitsel, O., Raisch, T., Prumbaum, D., et al. (2019). SPHIRE-crYOLO is a fast and accurate fully automated particle picker for cryo-EM. Commun Biol *2*, 218.

Weigand, M.R., Ashbolt, N.J., Konstantinidis, K.T., and Santo Domingo, J.W. (2014). Genome sequencing reveals the environmental origin of enterococci and potential biomarkers for water quality monitoring. Environ. Sci. Technol. *48*, 3707–3714.

Weigel, L.M., Clewell, D.B., Gill, S.R., Clark, N.C., McDougal, L.K., Flannagan, S.E., Kolonay, J.F., Shetty, J., Killgore, G.E., and Tenover, F.C. (2003). Genetic analysis of a high-level vancomycin-resistant isolate of Staphylococcus aureus. Science *302*, 1569–1571.

Wieczorek, M., Abualrous, E.T., Sticht, J., Álvaro-Benito, M., Stolzenberg, S., Noé, F., and Freund, C. (2017). Major Histocompatibility Complex (MHC) Class I and MHC Class II Proteins: Conformational Plasticity in Antigen Presentation. Front. Immunol. *8*, 292.

Wilke, G.A., and Bubeck Wardenburg, J. (2010). Role of a disintegrin and metalloprotease 10 in Staphylococcus aureus alpha-hemolysin-mediated cellular injury. Proc. Natl. Acad. Sci. USA *107*, 13473–13478.

Yamashita, K., Kawai, Y., Tanaka, Y., Hirano, N., Kaneko, J., Tomita, N., Ohta, M., Kamio, Y., Yao, M., and Tanaka, I. (2011). Crystal structure of the octameric pore of staphylococcal γ-hemolysin reveals the β-barrel pore formation mechanism by two components. Proc. Natl. Acad. Sci. USA *108*, 17314–17319.

Yamashita, D., Sugawara, T., Takeshita, M., Kaneko, J., Kamio, Y., Tanaka, I., Tanaka, Y., and Yao, M. (2014). Molecular basis of transmembrane beta-barrel formation of staphylococcal pore-forming toxins. Nat. Commun. *5*, 4897.

Yan, X.X., Porter, C.J., Hardy, S.P., Steer, D., Smith, A.I., Quinsey, N.S., Hughes, V., Cheung, J.K., Keyburn, A.L., Kaldhusdal, M., et al. (2013). Structural and functional analysis of the pore-forming toxin NetB from Clostridium perfringens. MBio *4*, e00019–e13.

Zaheer, R., Cook, S.R., Barbieri, R., Goji, N., Cameron, A., Petkau, A., Polo, R.O., Tymensen, L., Stamm, C., Song, J., et al. (2020). Surveillance of Enterococcus spp. reveals distinct species and antimicrobial resistance diversity across a One-Health continuum. Sci. Rep. *10*, 3937.

Zhang, K. (2016). Gctf: Real-time CTF determination and correction. J. Struct. Biol. *193*, 1–12.

Zhang, S., Lebreton, F., Mansfield, M.J., Miyashita, S.I., Zhang, J., Schwartzman, J.A., Tao, L., Masuyer, G., Martinez-Carranza, M., Stenmark, P., et al. (2018). Identification of a Botulinum Neurotoxin-like Toxin in a Commensal Strain of Enterococcus faecium. Cell Host Microbe *23*, 169–176.e6.

Zheng, S.Q., Palovcak, E., Armache, J.P., Verba, K.A., Cheng, Y., and Agard, D.A. (2017). MotionCor2: anisotropic correction of beam-induced motion for improved cryo-electron microscopy. Nat. Methods *14*, 331–332.

Zivanov, J., Nakane, T., Forsberg, B.O., Kimanius, D., Hagen, W.J., Lindahl, E., and Scheres, S.H. (2018). New tools for automated high-resolution cryo-EM structure determination in RELION-3. eLife *7*, e42166.

Please cite this article in press as: Xiong et al., Emerging enterococcus pore-forming toxins with MHC/HLA-I as receptors, Cell (2022), https://doi.org/10.1016/j.cell.2022.02.002

STAR★METHODS

KEY RESOURCES TABLE

REAGENT or RESOURCE	SOURCE	IDENTIFIER
Antibodies		
Mouse monoclonal anti-GST	Thermo Fisher	8-326, RRID:AB_2537630
Mouse monoclonal anti-HLA class I	Abcam	ab70328, RRID:AB_1269092
Rabbit monoclonal anti-B2M	Abcam	ab75853, RRID:AB_1523204
Mouse monoclonal anti-actin	Sigma	AC-15, RRID:AB_476970
Rabbit polyclonal anti-Epx2	This paper	N/A
Bacterial and virus strains		
Enterococcus strain DIV0147	This paper	N/A
Enterococcus strain DIV0391	This paper	N/A
Enterococcus strain 257EA1	This paper	N/A
E. coli BL21(DE3)	New England Biolabs	C2527
E. coli DH5-alpha	New England Biolabs	C2987
Biological samples		
Fresh human blood	Stemcell Technology	70508.2
Chemicals, peptides, and recombinant proteins		
All the other chemicals	Sigma	N/A
PolyJet	SignaGen	SL100688
PEIMax	Polysicences	24765-1
Polybrene	Santa Cruz	sc-134220
Dulbecco's Modified Eagle Medium	Cytiva,	SH30022
RPMI 1640 medium	Cytiva	SH30027
Fetal bovine serum	Life technologies	26140-079
Penicillin/streptomycin	Life technologies	15140-122
Puromycin	ThermoFisher	A1113830
Blasticidin S	RPI	B12150.01
Hygromycin B	EMD Millipore	400051
BHI medium	Thermo Scientific	CM1135B
Protease Inhibitor Cocktail	Roche	4693159001
Nitrocellulose membrane	GE Healthcare	10600002
DAPI-containing mounting medium	SouthernBiotech	0100-20
Autoinduction medium	ForMedium	AIMLB0210
biotin-labeled HLA-I complex	Eagle Biosciences	1001
biotin-labeled human FcRn complex	BPS Bio	71283
Rhodamine-dextran 70kDa	Sigma	R9379
Human IFN-γ	StemCell Technologies, Inc.	78141
Mouse IFN-γ	StemCell Technologies, Inc.	78021
Epx1	This paper	N/A
Epx2	This paper	N/A
Epx3	This paper	N/A
Epx4	This paper	N/A
GST-Epx2	This paper	N/A
GST-Epx3	This paper	N/A
GST-Epx4	This paper	N/A
B2M-Fc	This paper	N/A

(*Continued on next page*)

Please cite this article in press as: Xiong et al., Emerging enterococcus pore-forming toxins with MHC/HLA-I as receptors, Cell (2022), https://doi.org/10.1016/j.cell.2022.02.002

Continued

REAGENT or RESOURCE	SOURCE	IDENTIFIER
Critical commercial assays		
Gibson Assembly	NEB	E2621
BCA assay kit	ThermoFisher	23225
Genomic DNA extraction kit	QIAGEN	13323
PMBCs isolate kit	Stemcell Technology	19654
LDH release assay	Thermo Scientific	C20301
Deposited data		
Prepore structure of pore-forming toxin Epx1	PDB	PDB: 7T4E
Pore structure of pore-forming toxin Epx4	PDB	PDB: 7T4D
Experimental models: Cell lines		
HeLa	ATCC	CCL-2
A549	ATCC	CRM-CCL-185
5637	ATCC	HTB-9
U2OS	ATCC	HTB-96
Huh7	Y. Matsuura	N/A
HEK293T	ATCC	CRL-3216
HEK293	ATCC	CRL-1573
U937	ATCC	CRL-1593.2
Daudi	ATCC	CCL-213
CT26	ATCC	CCL-2638
Raw264.7	ATCC	TIB-71
Vero	ATCC	CCL-81
MDCK	ATCC	CCL-34
BMDM	Susan Carpenter	N/A
S2R+	DGRC	RRID:CVCL_Z831
HUVECs	Lonza	00191027
Expi293F	ThermoFisher	A14527
HeLa-B2M-KO-Mix	This paper	N/A
HeLa-HLA-A-KO-Mix	This paper	N/A
HeLa-GAGE1-KO-Mix	This paper	N/A
HeLa-SNX17-KO-Mix	This paper	N/A
Experimental models: Organisms/strains		
Cultured human intestinal organoids	Organoid core facility at Harvard Digestive Disease Center	N/A
Recombinant DNA		
Full-length Epx genes	Genewiz	Synthesized DNA
Full-length of mouse, equine, bovine, pig and rabbit B2M and HLA genes	Twist Bioscience	Synthesized DNA
Human B2M cDNA	GE Dharmacon	MHS6278-202758740
Human HLA-A cDNA	GE Dharmacon	MHS6278-202757462
Human HLA-B cDNA	GE Dharmacon	MHS6278-202804742
Human HLA-C cDNA	GE Dharmacon	MHS1010-202726224
pcDNA3.1	ThermoFisher	V80020
pET22b	Addgene	69744-3
pGEX4T1	Addgene	27458001
pMD2.G	Addgene	12259
pSPAX2	Addgene	12260
LentiGuide-puro	Addgene	52963

(*Continued on next page*)

Please cite this article in press as: Xiong et al., Emerging enterococcus pore-forming toxins with MHC/HLA-I as receptors, Cell (2022), https://doi.org/10.1016/j.cell.2022.02.002

Continued

REAGENT or RESOURCE	SOURCE	IDENTIFIER
Lenti-SpCas9 blast	Addgene	104997
GeCKO-V2 sgRNA library	Addgene	1000000049
Lentiguide-B2M	This paper	N/A
Lentiguide-HLA-A	This paper	N/A
Lentiguide-GAGE1	This paper	N/A
Lentiguide-SNX17	This paper	N/A
pGEX4T1-Epx2	This paper	N/A
pGEX4T1-Epx3	This paper	N/A
pGEX4T1-Epx4	This paper	N/A
pET22b-Epx1	This paper	N/A
pET22b-Epx2	This paper	N/A
pET22b-Epx3	This paper	N/A
pET22b-Epx4	This paper	N/A
pcDNA3.1-hB2M-FLAG	This paper	N/A
pcDNA3.1-hB2M-Fc	This paper	N/A
pcDNA3.1-hHLAA-FLAG	This paper	N/A
pcDNA3.1-hHLAB-FLAG	This paper	N/A
pcDNA3.1-hHLAC-FLAG	This paper	N/A
pcDNA3.1-pep-hB2M-FLAG	This paper	N/A
pcDNA3.1-hB2M-hHLAA-FLAG	This paper	N/A
pcDNA3.1-hB2M-hHLAB-FLAG	This paper	N/A
pcDNA3.1-hB2M-hHLAC-FLAG	This paper	N/A
pcDNA3.1-pep-hB2M-hHLAA-FLAG	This paper	N/A
pcDNA3.1-pep-hB2M-hHLAB-FLAG	This paper	N/A
pcDNA3.1-pep-hB2M-hHLAC-FLAG	This paper	N/A
pcDNA3.1-mB2M-mHLAC-FLAG	This paper	N/A
pcDNA3.1-boB2M-boHLAC-FLAG	This paper	N/A
pcDNA3.1-piB2M-piHLAC-FLAG	This paper	N/A
pcDNA3.1-rbB2M-rbHLAC-FLAG	This paper	N/A
pcDNA3.1-eqB2M-eqHLAC-FLAG	This paper	N/A
pcDNA3.1-MHC-hhhm-FLAG	This paper	N/A
pcDNA3.1-MHC-mmmh-FLAG	This paper	N/A
pcDNA3.1-MHC-hmmm-FLAG	This paper	N/A
pcDNA3.1-MHC-mhhh-FLAG	This paper	N/A
pcDNA3.1-MHC-hmmh-FLAG	This paper	N/A
pcDNA3.1-MHC-mhhm-FLAG	This paper	N/A
pcDNA3.1-B2M-FLAG	This paper	N/A
Software and algorithms		
OriginPro	OriginLab	v8.5
Excel	Microsoft	2007
BLItz pro. software	ForteBio	Version 1.1.0.29
ImageJ	https://imagej.nih.gov/ij/	Version 1.52o
Phenix	(Adams et al., 2010)	https://phenix-online.org/documentation/reference/refinement.html
Coot	(Emsley et al., 2010)	https://www2.mrc-lmb.cam.ac.uk/personal/pemsley/coot/
MotionCorr2 algorithm	SbGrid Consortium	(Zheng et al., 2017)
Relion3.1	SbGrid Consortium	(Zivanov et al., 2018)
Automated particle picking with crYOLO	SbGrid Consortium	(Wagner et al., 2019) Optimized in HMS facility

(*Continued on next page*)

Please cite this article in press as: Xiong et al., Emerging enterococcus pore-forming toxins with MHC/HLA-I as receptors, Cell (2022), https://doi.org/10.1016/j.cell.2022.02.002

Continued

REAGENT or RESOURCE	SOURCE	IDENTIFIER
DeepEMhancer	SbGrid Consortium	(Sanchez-Garcia et al., 2021)
UCSF-Chimera	UCSF Resource for Biocomputing, Visualization, and Informatics, NIH	https://www.cgl.ucsf.edu/chimera/
Pymol	SchÖdinger, LLC	https://pymol.org/2/
Other		
Applied Photo-physics Chirascan plus spectropolarimeter	Jasco	J-815
Microplate reader	BMG Labtech	FLUOstar Omega
Fluorescence microscope	Olympus	IX51
Spinning Disk Confocal Microscope	Olympus	DSU-IX81
Fuji LAS3000 imaging system	Fuji	LAS3000
Personal assay BLItz System	ForteBio	BLItz System
Streptavidin (SA) Biosensors	ForteBio	18-5060
Tecnai G2 Spirit BioTWIN electron microscope and recorded with an AMT 2k CCD camera	Harvard Medical School Electron Microscopy Facility	N/A

RESOURCE AVAILABILITY

Lead contact

Further information and requests for resources and reagents should be directed to and will be fulfilled by the lead contact, Min Dong (min.dong@childrens.harvard.edu).

Materials availability

All materials used in the study are available to any researcher for purposes of reproducing or extending the analysis.

Data and code availability

- All data supporting the findings of this study are available within the paper or from the corresponding author upon request. Structures of Epx1 (PDB ID: 7T4E) and Epx4 (PDB ID: 7T4D) have been deposited into the Protein Data Bank (PDB).
- This paper does not report original code.
- Any additional information required to reanalyze the data reported in this paper is available from the lead contact upon request.

EXPERIMENTAL MODEL AND SUBJECT DETAILS

Cell lines and organoids

All the cells were cultured in DMEM media plus 10% fetal bovine serum (FBS) and 100 U penicillin / 0.1 mg/mL streptomycin in a humidified atmosphere of 95% air and 5% CO_2 at 37°C. Cultured human intestinal organoids were provided as de-identified materials from the organoid core facility at Harvard Digestive Disease Center.

Bacterial strains

Strain *E. faecalis* 257EA1 is derived from commercial chicken meat as reported (Manson et al., 2019). *E. faecium* DIV0147 was recovered from presumptive horse feces on a remote trail in Montana, USA. Culture of enterococci and purification, short read sequencing, assembly, and annotation of genomic DNA were performed essentially as described (Manson et al., 2019). *E. faecium* DIV0391 was isolated from crow feces in Berlin, Germany (GenBank: GCA_002141075.1)

METHOD DETAILS

Enterococcus isolation, sequencing, and bioinformatics analysis

The enterococcal diversity project is an ongoing collaboration between M.S.G. (Harvard Medical School) and A.M.E. (Broad Institute of MIT and Harvard), with the goal of surveying the global diversity of *Enterococcus* to understand the biological basis for host association and antibiotic resistance transmission through comparative genomics.

Long read sequencing was performed using an Oxford Nanopore MinION Mkl (Oxford Nanopore Technologies). Hybrid assembly of these reads with quality-trimmed 2 × 150bp NextSeq Illumina reads was then performed using SPAdes 3.8.0 with default options,

Please cite this article in press as: Xiong et al., Emerging enterococcus pore-forming toxins with MHC/HLA-I as receptors, Cell (2022), https://doi.org/10.1016/j.cell.2022.02.002

except for–nanopore–only-assembler–k 25,35,45,55,65,75. Scaffolds < 1000 bp were removed from the assembly. Epx1 and Epx2 were first discovered using a systematic analysis of enterococcal proteins of unknown function using the protein modeling and prediction tool (default parameter) Phyre2 (Kelley et al., 2015), which revealed structural homology to *S. aureus* leukocidin and beta and delta toxins from *C. perfringens*. Epx3 to 8 were discovered using blastp with Epx 1 and 3 as query sequences against the nr database with default parameters (BLOSUM62, gap existence = 11, gap extension = 1, with conditional compositional score matrix adjustment). Epx sequences representing all major types (1-8) were aligned in a multiple alignment using ClustalO (v1.2.1), then pairwise identity between all toxins was calculated in a 50-amino-acid sliding window across the length of the multiple alignment with a step of 1.

The 16S rRNA based phylogeny for the *Enterococcus* genus was extracted from the All-Species Living Tree project and edited using iTOL (Letunic and Bork, 2016). The core genome, SNP-based phylogenetic tree of *E. faecalis*, *E. faecium*, and *E. hirae*, was constructed using RAxML and a concatenated alignment of 1513, 1144 and 1891 single-copy core orthogroups, respectively. The 1000 bootstrap iterations were calculated using the rapid bootstrapping algorithm of RAxML. The presence of antibiotic resistance genes and plasmid predictions were determined using available online tools (PlasmidFinder and Resfinder https://cge.cbs.dtu.dk/services). Plasmid sequences were compared and visualized as a circular alignment using CGView (Stothard et al., 2019).

Cell lines and antibodies

The following cell lines were originally obtained from ATCC: HeLa (CCL-2), A549 (CRM-CCL-185), 5637 (HTB-9A), U2OS (HTB-96), HEK293T (CRL-3216), HEK293 (CRL-1573), U937 (CRL-1593.2), Daudi (CCL-213), CT26 (CCL-2638), Raw264.7 (TIB-71), Vero (CCL-81), and MDCK (CCL-34). The Huh7 cell line was provided by Y. Matsuura. The BMDM cell line was provided by Susan Carpenter. The S2 cell line was originally obtained from DGRC (RRID:CVCL_Z831). HUVECs were from pooled donors and purchased from Lonza. Anti-FLAG mouse monoclonal antibody (M2) and anti-actin mouse monoclonal antibody (AC-15) were purchased from Sigma. Mouse monoclonal antibody against GST (8-326) was purchased from Thermo Fisher. Mouse monoclonal antibody against HLA Class 1 ABC (ab70328) and rabbit monoclonal antibody against B2M (ab75853) were purchased from Abcam.

Constructs

The full-length genes of Epxs were synthesized by Genewiz. The constructs for expressing Epxs and GST-Epxs were generated by sub-cloning Epx1 (residues 24-345), Epx2 (residues 30-334), Epx3 (residues 24-329), and Epx4 (residues 32-335) into the pET22b (Addgene, 69744-3) vector with a C-terminal His6 tag or the pGEX4T1 (Addgene, 27458001) vector with a N-terminal GST tag. Mutant Epxs were generated by site-directed mutagenesis and verified by sequencing. The cDNAs of HLA-I were originally obtained from GE Dharmacon: B2M (MHS6278-202758740); HLA-A (MHS6278-202757462); HLA-B (MHS6278-202804742) and HLA-C (MHS1010-202726224). The full-length genes of murine, equine, bovine, and porcine B2M and MHC-I α-subunit genes were synthesized by Twist Bioscience. The full-length B2M, full-length HLA, and B2M-HLA fusion constructs (full length B2M with linker (GGGGS) x 3 fused with HLA-A (residues 25-365), HLA-B (residues 25-362), or HLA-C (residues 25-366), with an additional human Fc tag or a triple-FLAG tag at their C-termini (with EFGSGSGS linker)) were cloned into pcDNA3.1 vector (Invitrogen, V800-20) via Gibson Assembly (NEB, E2621). The representative antigen peptide (HER2 residues 63-71, TYLPTNASL) and the linker (GGGGS) x 3 were synthesized and inserted into the B2M-HLA fusion constructs via Gibson Assembly. The human and mouse HLA/MHC chimeric proteins were constructed as follows: mhhh (mB2M - (GGGGS) × 3 – hHLA no signal (25-365)), hhhm (hB2M - (GGGGS) × 3 - hHLA-A α1+α2 (25-206) - mH2K α3+TM (205-369)), mhhm (mB2M - (GGGGS) × 3 - hHLA-A α1+α2 (25-206) - mH2K α3+TM (205-369)), mmmh (mB2M - (GGGGS) × 3 - mH2K α1+α2 (22-203) - hHLA-A α3+TM (207-365)), hmmh (hB2M - (GGGGS) × 3 - mH2K α1+α2 (22-203) - hHLA-A α3+TM (207-365)), hmmm (hB2M - (GGGGS) × 3 - mH2K no signal (22-369)), with an EFGSGSGS linker and a triple-FLAG tag at their C-termini. These constructs were cloned into pcDNA3.1 vector via Gibson Assembly.

Protein purification

Epxs were expressed recombinantly with either a C-terminal His6 tag in the pET22b vector or N-terminal GST tag in pGEX4T1 vector in *E. coli* strain BL21 (DE3) at 20°C for 16 h using autoinduction medium (ForMedium AIMLB0210). Bacteria were harvested and resuspended in protein purification buffer (PP buffer) containing 200 mM NaCl, 20 mM Tris pH 7.5, 10% (v/v) glycerol, and then lysed by sonication and centrifugation. For GST-tagged proteins, bacterial lysates were applied to GSTrap columns (GE Healthcare) equilibrated with PP buffer. After washing with PP buffer, bound proteins were eluted using PP buffer containing 10 mM reduced glutathione (Sigma-Aldrich), pH 7.5. For His6 tagged proteins, bacterial lysates were applied to HisTrap (GE Healthcare) nickel columns equilibrated with PP buffer, and columns were washed with PP buffer containing 20 mM imidazole. Bound proteins were eluted using PP buffer with a linear imidazole gradient from 20 mM to 500 mM. The proteins were further purified through HiTrap Q ion-exchange and HiLoad 16/60 Superdex 75 (GE Healthcare) gel filtration columns using the buffer containing 200 mM NaCl, 20 mM Tris pH 7.5. Proteins were concentrated using Vivaspin protein concentrator column (GE Healthcare) to ~10 mg/mL.

Cell viability assay (MTT assay)

Cells were plated in 96-well microplates overnight to ~70% confluence and then exposed to 2-fold serial dilutions of toxins in medium for 4 h at 37°C. MTT (0.5 mg/mL, Research Products International M92050) was added to each well and incubated for 4 h at 37°C. A total of 100 μL solubilization solution (10% SDS in 0.01 M HCl) was then added to each well, incubated overnight

at room temperature, and the absorbance of formazan was then measured at 580 nm using a microplate reader (BMG Labtech, FLUOstar Omega). A vehicle control without toxins was analyzed in parallel. The cell viability curves were analyzed and fitted using Origin software (version 8.5). The toxin concentration that induced 50% of cells to lose viability is defined as the IC_{50} value. Data were represented as mean ± SD from three independent biological replicates. Data were considered significant when p-value < 0.01 (Student's t test, double-tail). Statistical analysis was performed using Excel.

Liposome leakage assay

Liposomes were produced using POPC: PE: cholesterol at a molar ratio of 4:3:3 (Avanti polar lipids). Briefly, these lipids were dried and then rehydrated in PBS buffer together with 10 mM sulforhodamine B, incubated for 30 min at 37°C, followed by vigorous vertexing. The suspension was frozen in liquid nitrogen, followed by thawing at 37°C for 5 rounds. The lipid suspension was then extruded through a 100 nm pore filter 21 times to produce liposomes, which then went through G25 desalting column to remove free dyes. The dye leakage assay was carried out by mixing toxins with 80 μL liposomes and incubating at 37°C. Sulforhodamine B release was measured every 20 s with excitation/emission wavelengths at 545/590 nm. The detergent Triton X-100 (4%, v/v) was utilized to break all liposomes to quantify the maximal signal of sulforhodamine B, which is set as 100% leakage.

Negative staining EM of liposomes

Liposome-bound Epx2 samples were prepared by mixing liposome containing POPC: PE: cholesterol at a molar ratio of 4:3:3 with 2 μM Epx2 at 37°C for 30 min. We placed formvar-carbon coated grid (Electron Microscopy Sciences) with carbon side up in the Glow Discharge System at 30 mA for 30 s. 10 μL of liposome-bound Epx2 was then applied to freshly glow-discharged grid, incubated for 30 s, washed twice with H_2O and blotted by touching filter paper. The samples were then negatively stained with 2% (w/v) aqueous uranyl acetate for 1 min and air-dried. The grids were then imaged using a Tecnai G2 Spirit BioTWIN electron microscope and recorded with an AMT 2k CCD camera (Harvard Medical School Electron Microscopy Facility).

Oligomerization assay

20 μL of Epxs (25 μM) proteins were mixed with 80 μL of liposomes containing POPC: PE: cholesterol at a molar ratio of 4:3:3. The mixtures were then incubated at 37°C for 1 h. Liposome-bound Epxs were solubilized using 20 μL of protein loading buffer (375 mM Tris-HCl, 9% SDS 50% glycerol, and 0.03% bromophenol blue). Samples were analyzed by 4%–20% SDS-PAGE and Coomassie blue staining to detect SDS-resistant oligomerization bands.

Planar lipid bilayer electrophysiology

Planar lipid bilayer electrophysiology experiments were carried out using MECA chips (50 μm) on an Orbit Mini apparatus (Nanion). The lipid bilayer was painted with 50% DPhPc, 30% DOPE, and 20% DOPS at 5 mg/mL in n-octane. Purified Epx1 was added at 1 μg/mL. Once pore-formation events were detected, excess Epx1 was slowly removed by buffer exchange using a perfusion system (Eastern Scientific LLC). Experiments were carried out in 10 mM Tris-HCl, pH 7, 100 mM NaCl and recorded at 1.25 kHz, filtered at 625 Hz and analyzed in Clampfit 10. Average channel currents were derived from three independent measurements.

Pore size was calculated using the equation: $\frac{1}{\gamma} = \left(l + \frac{\pi r}{2}\right)\frac{\rho}{\pi r^2}$,

where γ is the pore conductance, r is the radius, l is the length of the pore (10 nm), and ρ is the resistivity of the buffer (100 Ω·cm).

Circular dichroism spectroscopy

Purified wild-type Epxs and mutants were diluted to 0.5 mg/mL in PBS. Circular dichroism spectra were recorded at 20°C using an Applied Photo-physics Chirascan plus spectropolarimeter (Jasco J-815) with a 1 mm path-length cell and a bandwidth of 1 nm. Spectra were scanned from 190 to 260 nm with a step-size of 1 nm and were repeated five times. Each reported circular dichroism curve was the average of five scans. Protein concentrations were determined with their 280 nm absorbance.

Crystallization, data collection, and structure determination

Crystallization was performed using the sitting drop vapor diffusion method at 4°C by mixing equal volumes (0.2–1.0 μL) of Epx4 with the reservoir solution. Crystals were grown in 5% (w/v) polyethylene glycol 8,000, 40% (v/v) MPD, 0.1 M Sodium Cacodylate, pH 6.5. Crystals were briefly soaked in cryoprotectant solution containing reservoir solution supplemented with 10% (v/v) glycerol and flash-frozen in liquid nitrogen for data collection at the Advanced Photon Source using Northeastern Collaborative Access Team (NE-CAT) beamlines 24-ID-C and 24-ID-E.

All diffraction images were indexed, integrated, and merged using HKL2000 (Otwinowski and Minor, 1997). The structure was determined by molecular replacement using MOLREP (Vagin and Teplyakov, 2010) with the delta toxin structure (PDB ID: 2YGT) (Huyet et al., 2013) as the search model. Structural refinement was carried out using PHENIX (Adams et al., 2010), and iterative model building was performed in *Coot* (Emsley et al., 2010). Structural figures were generated using the PyMOL (https://www.pymol.org:443/) program. Detailed data collection and refinement statistics are provided in Table S3.

Please cite this article in press as: Xiong et al., Emerging enterococcus pore-forming toxins with MHC/HLA-I as receptors, Cell (2022), https://doi.org/10.1016/j.cell.2022.02.002

Cryo-EM data collection and analysis

A 4 μL drop of Epx1 protein at 1 mg/mL was applied to a glow-discharged Quantifoil grid (R 1.2/1.3 400 mesh, copper, Electron Microscopy Sciences) and blotted once for 6 s after a wait time of 15 s in 100% humidity at 4°C and plunged into liquid ethane using an FEI Vitrobot Mark IV. Cryo-EM datasets were collected at 300 kV on a Titan Krios microscope (FEI) at the Harvard Cryo-Electron Microscopy Center for Structural Biology. Movies (50 frames, each 0.04 s, total dose 53.54 e/Å^2) were recorded using a K3 detector (Gatan) with a defocus range of −1.5 to −2.5 μm. Automated single-particle data acquisition was performed with SerialEM, with a nominal magnification of 105,000 × in counting mode, which yielded a calibrated pixel size of 0.825 Å.

Raw movies were motion-corrected using MotionCor2 (Zheng et al., 2017) and combined into micrographs, yielding 4,920 Epx1 micrographs used for image processing. The defocus value for each micrograph was determined using Gctf (Zhang, 2016). 1,963,299 particles were boxed using crYOLO (Wagner et al., 2019). Chosen particles were extracted from micrographs and binned two times (pixel size 1.65 Å) in RELION 3.1 (Zivanov et al., 2018). 2D classification was performed to discard bad particles. Good class averages were selected for the reconstruction of an initial model in RELION 3.1. 1,680,746 particles were selected for 3D classification. C1 symmetry was used for the first round of 3D classification. 800,275 particles likely representing assembly intermediates (including heptamers) and 150,842 octamer particles were selected for further processing. A round of 3D classification with C8 symmetry was performed to discard bad particles. 119,503 particles were selected for the final reconstruction. With C8 symmetry, the resolution of the Epx1 octamer map is 3.14 Å using the "gold" standard Fourier shell correlation (FSC) = 0.143 criterion. After CTF refinement and Bayesian polishing, the resolution of the final map improved to 2.87 Å. DeepEMhancer was applied to improve the map's resolution at the top domain (Sanchez-Garcia et al., 2021). The local resolution distribution of the map was determined by ResMap (Kucukelbir et al., 2014).

To generate an initial model, we docked the Epx4 X-ray crystal structure into the map as a rigid body using Chimera (Pettersen et al., 2004). This was followed by iterative model building in *Coot* (Emsley et al., 2010). PHENIX (Adams et al., 2010) was used to refine the model by iterative positional and B-factor refinement in real space. Data collection and refinement statistics are provided in Table S4.

Genome-wide CRISPR-Cas9 screen and generating KO cells

HeLa cells that stably express Cas9 (HeLa-Cas9) were generated using lentivirus (LentiCas9-Blast, Addgene, #52962) and selected using 10 μg/mL blasticidin S (RPI, B12150.01). The GeCKO-V2 sgRNA library was obtained from Addgene (#1000000049). The sub-library A and B were independently packed into lentivirus. HeLa-Cas9 Cells were transduced with sgRNA lentiviral libraries at a MOI (multiplicity of infection) of 0.3. Infected cells were selected with 5 μg/mL puromycin (Thermo Scientific, A1113830) for one week. 3.3 × 10^7 cells for sub-library A or 2.9 × 10^7 cells for sub-library B were plated onto 15-cm culture dishes to ensure enough sgRNA coverage, with each sgRNA being represented 500 times. These cells were either saved as initial library control or exposed to 0.25 μg/mL Epx for 24 h. The surviving cells were washed and re-seeded within toxin-free medium until ~70% confluence, followed by the next round of selection with 0.5 μg/mL Epx for 24 h. The genomic DNA of surviving cells was extracted using a commercial kit (QIAGEN, 13323). The DNA fragments containing the sgRNA sequences were amplified by PCR using primers lentiGP-1_F (AAT GGACTATCATATGCTTACCGTAACTTGAAAGTATTTCG) and lentiGP-3_R (ATGAATACTGCCATTTGTCTCAAGATCTAGTTACGC). Next-generation sequencing was performed by a commercial vendor (Genewiz, Illumina HiSeq). The selected sgRNA sequences (B2M: CAGTAAGTCAACTTCAATGT; HLA-A: TCCCTCCTTACCCCATCTCA; GAGE1: GGGTCCATCTCCTGCCCATC; SNX17: CTTT CAACAGTTTCCTGCGT) were cloned into The LentiGuide-Puro vector (Addgene, #52963). The KO cells were generated via lentiviral transduction of sgRNAs into HeLa-Cas9 cells. Mixed populations of transduced cells were selected with puromycin (5 μg/mL).

Cell surface binding and immunostaining

Cells were seeded onto glass coverslips (Hampton, HR3-239) and exposed to GST-Epx2 or GST-Epx3 (50 μg/mL) on ice for 60 min. Cells were washed three times with ice-cold PBS, fixed with 4% paraformaldehyde (PFA,w/v) for 20 min, blocked with 10% goat serum for 40 min, followed by incubation with primary antibodies against GST (1:500 dilution) for 1 h and fluorescence-labeled secondary antibodies for 1 h. Slides were sealed within DAPI-containing mounting medium (SouthernBiotech, 0100-20). Fluorescence images were captured with an Olympus DSU-IX81 spinning disk confocal system. Images were pseudo-colored and analyzed using ImageJ (Version 1.52o).

Pull-down and immunoblot analysis

Cell lysates were harvested in 1 mL lysis buffer (PBS, 1% Triton X-100, 0.1% SDS, plus a protease inhibitor cocktail (Sigma-Aldrich), 1 mL per 10-cm dish) and incubated with 20 μg GST-tagged Epx proteins for 4 h at 4°C. Pull-down experiments were carried out using 15 μL glutathione agarose beads, washed, pelleted, and boiled. Samples were subjected to SDS-PAGE analysis and transferred onto a nitrocellulose membrane (GE Healthcare, 10600002). The membrane was blocked (10 mM Tris, pH 7.4, 150 mM NaCl, 0.1% Tween-20, 5% skim milk) for 40 min, followed by incubation with primary antibodies for 1 h and secondary antibodies for another 1 h, and then analyzed using the enhanced chemiluminescence method (Thermo Fisher Scientific, 34080). Blot images were taken using a Fuji LAS3000 imaging system. Images were analyzed using ImageJ (Version 1.52o).

Biolayer interferometry (BLI) assays

The binding between Epx2 and HLA-I complex was measured using the BLI assay with the BLItz system (ForteBio). Briefly, 10 μg/mL biotin-labeled HLA-I complex (Eagle Biosciences, #1001) or FcRn complex (BPS Bio, #71283) were immobilized onto capture biosensors (Streptavidin (SA) Biosensors, ForteBio) and washed with DPBS containing 0.5% BSA (w/v). Empty biosensors served as a control. These biosensors were then exposed to variable concentrations of GST-Epx2 in solution (GST-Epx2 binding), followed by washing (dissociation) in DPBS (0.5% (w/v) BSA). Binding affinities (K_D) were estimated using the BLItz software (ForteBio). The experiments were repeated three times.

IFN-γ treatment

Human and mouse IFN-γ (StemCell Technologies, Inc., #78141, #78021) powders were dissolved in PBS at a concentration of 0.1 mg/mL, and aliquoted and frozen at −20°C. Human and mouse cells were seeded into plates (96-well plates for cell viability assay and 6-well plates for immunoblots) and grew to ~70% confluence. Human and mouse organoids were seeded in 24-well plates. IFN-γ stock was diluted 10,000-folds into culture medium at a final concentration of 10 ng/mL and cells were incubated with medium containing IFN-γ for 20 h at 37°C. For cell viability assays, Epxs were added directly to IFN-γ-treated cells without changing medium.

Human umbilical vein endothelial cells (HUVECs) and mouse endothelial cells (mECs)

HUVECs were purchased from Lonza and cultured in the 0.2% gelatin-coated plates with complete endothelial cell growth media: 40% F-12K medium (Corning), 40% DMEM medium (Corning), 20% fetal bovine serum (FBS, Thermo Fisher Scientific), 1% homemade bovine brain food, 0.2% Heparin (Sigma-Aldrich, 50mg/mL), 1% penicillin streptomycin (GIBCO), and 0.1% ciprofloxacin (Corning, 12.5 mg/mL). Primary mECs were isolated from the lungs of 8~10-week-old C57BL/6J mice. Briefly, finely minced lung was digested with enzyme solution (2 mg/mL collagenase I, 5 mg/mL dispase, Roche) at 37°C for 45 min and filtered through a 70 μm cell strainer. The suspended cells were then centrifuged at 1200 rpm at 4°C for 8 min. The cell pellet was resuspended and centrifuged at 1200 rpm for 10 min, and the supernatant was removed. Anti-mouse CD31 MicroBeads (10 μL, Miltenyi Biotec) were added into 10^7 cells in 90 μL of buffer (PBS, pH 7.2, 0.5% BSA, and 2 mM EDTA). The cells were then mixed and incubated for 15 min at 4°C. After incubation, the cells were washed with the buffer described above. Mouse $CD31^+$ endothelial cells were isolated using an MS column and separator (Miltenyi Biotec), and then immediately seeded into pre-coated cell culture plates. Both HUVECs and mECs were used between passages 2 and 5.

Human intestinal organoids

Cultured human intestinal organoids were provided as de-identified materials from the organoid core facility at Harvard Digestive Disease Center. These organoids are originally from de-identified endoscopic biopsy samples from pediatric patients undergoing esophagogastroduodenoscopy at Boston Children's Hospital. All methods were approved by the Institutional Review Board of Boston Children's Hospital (Protocol number IRB-P00000529). To isolate crypts, biopsies were digested in 2 mg/mL of Collagenase Type I (Life Technologies, 17018029) reconstituted in Hank's Balanced Salt Solution for 40 min at 37°C. Samples were then agitated by pipetting followed by centrifugation at 500 g for 5 min at 4°C. The crypts were resuspended in 200-300 μL of Matrigel (Corning, 356231) with 50 μL plated onto 4-6 wells of a 24-well plate and polymerized at 37°C.

Isolated crypts were grown in Matrigel with organoid growth medium, which contains (v/v): L-WRN conditioned media (50%), DMEM/F12 (45%), Glutamax (1%), N-2 supplement (1%), B-27 supplement (1%), HEPES (10 mM), primocin (100 μg/mL), normocin (100 μg/mL), A83-01 (500 nM), N-acetyl-cysteine (500 μM), recombinant murine EGF (50 ng/mL), human [Leu15]-Gastrin I (10 nM), nicotinamide (10 mM), and SB202190 (10 μM). The medium was changed every two days. After 6-8 days of culture, the medium was removed and Cell Recovery Solution (Corning, 354253) was added. The plate was incubated at 4°C for 1 h. The Matrigel was mechanically resuspended and centrifuged at 500 g at 4°C for 5 min. The pelleted organoids were resuspended in fresh Matrigel and mechanically disrupted by pipetting up-and-down. The suspension was seeded into a fresh 24-well plate at 50 μL per well. After incubation at 37°C for 10 min, 500 μL of pre-warmed organoid growth media was added. After 2 days in culture, the organoids were changed to fresh media with IFN-γ and cultured overnight. Then, serial dilutions of toxins were added to the organoids for 4 h treatment. Cell viability was measured using the MTT assay.

Generation of a rabbit polyclone Epx2 antibody

A mutant inactive form of Epx2 (K50E/K56E, 5 mg) was purified in *E. coli* and utilized to immunize rabbits following a standard 3-month immunization protocol by a commercial vendor (Boston Molecules Inc., Boston, MA). Final bleeds were collected, and polyclonal antibodies were purified using a protein G column. ELISA assays were carried out to confirm the antibody titer against Epx2 (K50E/K56E). Antibodies purified with a protein G column from naive rabbits were used as the control IgG.

Culture of *E. faecium* and testing the toxicity of supernatants

E. faecium DIV0147 and DIV0391 were recovered from glycerol stock and grown overnight in 2 mL BHI medium (Thermo Scientific, CM1135B) 37°C in a shaker, followed by sub-culture (1:200 dilution) in 5 mL BHI medium for 48 h until the O.D. reached ~2.5. Culture supernatant was collected and concentrated ~75-fold using a protein concentrator (MilliporeSigma, UFC801008). HeLa cells were cultured in 96-well plates to ~70% confluence. Concentrated supernatant (20 μl per well) was then added to cell culture

medium (100 μl per well) and incubated for 30 min. Cells were then imaged using an Olympus microscope. For antibody neutralization assays, Epx2 antibody or control IgG (1 μg, 1:50 dilution) was added to each well immediately before adding the concentrated supernatant.

Co-culture with HeLa and U937 cells

E. faecium DIV0147 and DIV0391 were cultured in 5 mL BHI medium for 48 h until the O.D. reached ~2.5. Cells were cultured in 96-well plates (~75,000 cells per well) in standard DMEM cell culture medium (Cytiva, #SH30022) plus 10% fetal bovine serum (FBS) without antibiotics. A standard curve between O.D. and bacterial colony-forming units (CFUs) was generated by serial dilution and plating. Bacterial numbers were then quantified based on this O.D.-CFU standard curve. Bacteria were added to cell culture medium with a multiplicity of infection (MOI) at 800 and cultured together with cells for 6 h at 37°C. Cells were washed with PBS three times and subjected to MTT assays. For antibody neutralization assays, Epx2 antibody or control IgG (2 μg, 1:25 dilution) were added to each well immediately before adding the bacteria.

Co-culture with PBMCs and LDH release assays

Fresh human blood was purchased from a commercial vendor (Stemcell Technology, Cambridge, MA, #70508.2). PBMCs were isolated using a kit following supplier's instructions (Stemcell Technology, Cambridge, MA, #19654). PBMCs were seeded into a 96-well plate (~150,000 per well) and cultured using RPMI 1640 medium (Cytiva, #SH30027) plus 2% FBS without antibiotics. IFN-γ (StemCell Technologies, Inc., #78141, 10 ng/mL) was added to the medium. Bacteria were added to cell culture medium with a MOI at 800 and cultured together with cells for 4 h at 37°C. Cell culture supernatants were collected and subjected to LDH release assays using a commercial kit following the manufacturer's instructions (Thermo Scientific, #C20301). LDH release from 2% Triton X-100 treatment served as a positive control and was used as 100% to normalize other measurements. For antibody neutralization assays, Epx2 antibody or control IgG (2 μg, 1:25 dilution) was added to each well immediately before adding the bacteria.

Co-culture with intestinal organoids and dye leakage assays

Human intestinal organoids were obtained and cultured as described above. Trans-wells (Corning, 3470) were pre-coated with 200 μL of 10% Collagen (rat tail collagen type I, 3.90 mg/mL, Corning, 354236) in PBS for 2 h at 37°C followed by rinsing with PBS. To seed a single trans-well, organoids from 2-4 wells of a 24-well plate were recovered from Matrigel by incubation in cell recovery solution (Corning, 354253) for 20 min on ice and pooled. Following centrifugation at 500 g for 5 min at 4°C, the pellet was resuspended in 1X TriplE Express (GIBCO, #12605-010) for 10 min at 37°C. At the midpoint of this incubation, a bent P1000 tip was used to mechanically disrupt the pellet followed by pipetting up and down 50 times at the conclusion of the incubation. Chilled medium was then added to dilute the TriplE Express followed by centrifugation at 500 g for 5 min. The pellet was resuspended in organoid growth medium at a concentration of ~1.5-3.0 × 10^5 cells per 200 μL, seeded in pre-coated trans-wells and cultured at 37°C for ~7 days. Once confluent, monolayers were switched to antibiotic-free media containing 5% FBS, which contains (v/v): L-WRN conditioned media (25%), DMEM/F12 (70%), Glutamax (1%), N-2 supplement (1%), B-27 supplement (1%), HEPES (10 mM), A83-01 (500 nM), N-acetyl-cysteine (500 μM), recombinant murine EGF (50 ng/mL), human [Leu15]-Gastrin I (10 nM), nicotinamide (10 mM), and SB202190 (10 μM).

Cells were then stimulated with IFN-γ (10 ng/mL) for 16 h. Bacterium was added to cell culture medium with MOI at 800 and co-cultured with the cells for 6 h at 37°C. Cell culture supernatant was collected and subjected to LDH release assay. Cells were washed with PBS 3 times and subjected to permeability measurements using Rhodamine-dextran 70 kDa (Sigma, R9379). Briefly, Rhodamine-dextran was dissolved in P buffer (10 mM HEPES, pH 7.4, 1 mM sodium pyruvate, 10 mM glucose, 3 mM $CaCl_2$, 145 mM NaCl) or P/EGTA buffer (10 mM HEPES, pH 7.4, 1 mM sodium pyruvate, 10 mM glucose, 145 mM NaCl, 2 mM EGTA).

To measure the paracellular flux, the upper, and lower cell culture media were replaced with P buffer containing Rhodamine-dextran (1 mg/mL) and P buffer alone, respectively. P/EGTA buffer containing Rhodamine-dextran (1 mg/mL) and P/EGTA buffer were used as positive controls. After incubation for 4 h, the amounts of Rhodamine-dextran in the basolateral media were measured with a fluorometer (excitation at 530 nm and emission at 590 nm). Data are expressed as fluorescent intensity. For antibody neutralization assays, Epx2 antibody or control IgG (2 μg, 1:25 dilution) was added to each well before adding the bacterium.

Mass spectrometry analysis

The concentrated bacterial culture supernatants were analyzed by SDS-PAGE and Coomassie blue staining. The area around the size of Epx2 was cut into small pieces (about 1mm x 1mm x 1mm). These gel pieces were de-stained with de-staining buffer (25 mM NH_4HCO_3, 50% ACN), rinsed twice with acetonitrile, dried using speed-vac, then reduced with DTT and alkylated with iodoacetamide. Gel pieces were digested with trypsin at 37°C overnight. Digestion was terminated by adding 1 μL of 10% trifluoroacetic acid solution, and peptides were extracted twice with extraction buffer (50% acetonitrile, 0.1% formic acid). Extracted supernatants were concentrated using speed-vac and desalted with home-made C18 stage-tips. Elution from stage-tips was dried using speed-vac and reconstituted with sample buffer (2% acetonitrile, 0.1% formic acid). Samples were then subjected to LC-MS/MS analysis.

Please cite this article in press as: Xiong et al., Emerging enterococcus pore-forming toxins with MHC/HLA-I as receptors, Cell (2022), https://doi.org/10.1016/j.cell.2022.02.002

QUANTITATION AND STATISTICAL ANALYSIS

All quantitative data were analyzed and graphed using OriginPro 9.1 software. All data are represented as mean ± SD calculated using the OriginPro 9.1 software, unless indicated otherwise. Statistical details of the experiments are provided in the respective figure legends and in each methods section pertaining to the specific technique applied.

Supplemental figures

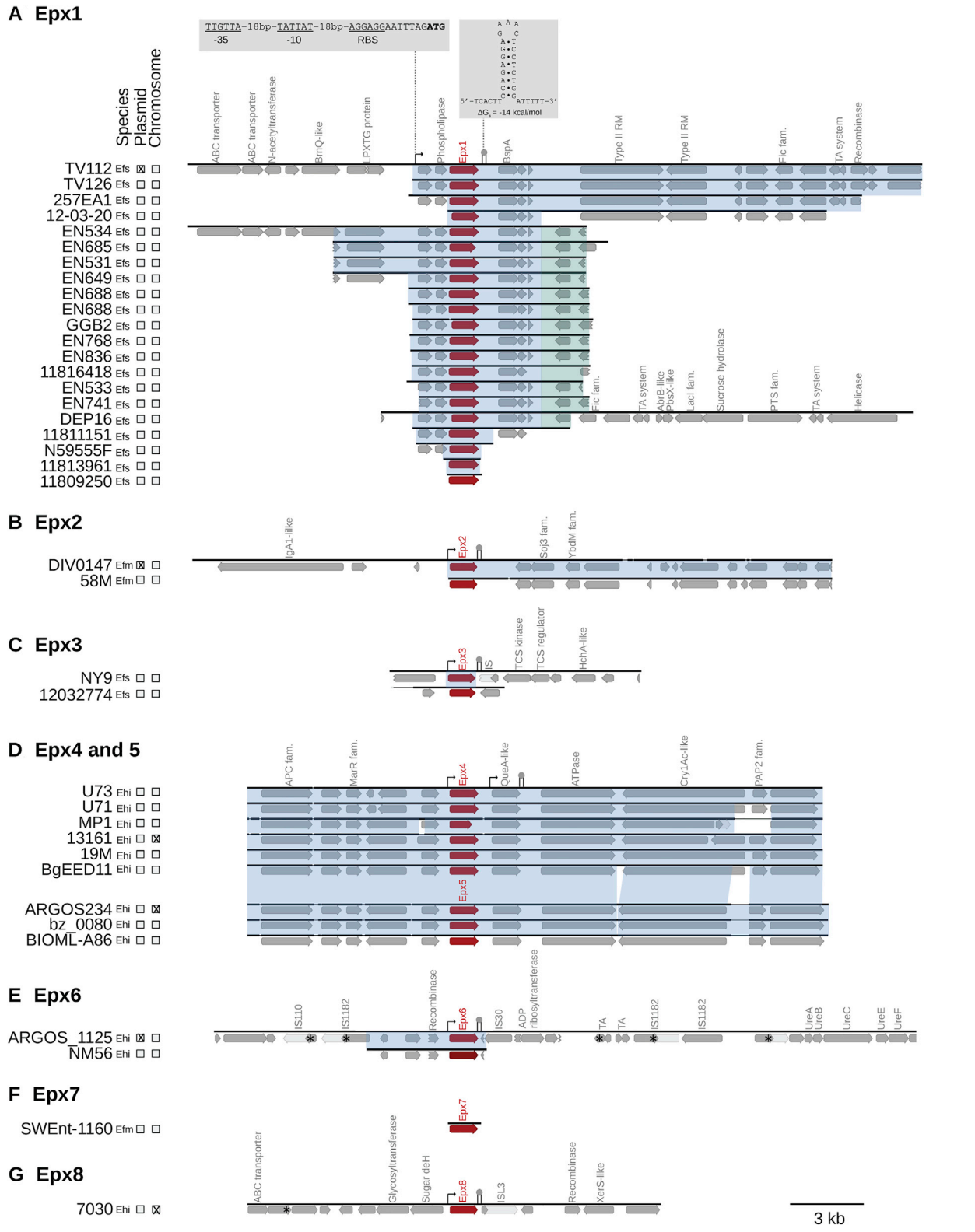

(legend on next page)

Figure S1. Analysis of the *epx* loci, related to Figure 1

The *epx*-carrying contigs were retrieved from publicly available draft genomes. When applicable, putative ORFs function (or homologous proteins), promoters and transcriptional terminators (predicted only for adjacent regions of *epx*) were indicated. For *epx1*, the specific sequence of the upstream promoter and downstream terminator (the computed ΔG_S free energy value of the stem-loop structure is indicated) are shown. For complete genomes only, the chromosomal or plasmidic location of the *epx* locus is indicated. For genomes with high quality, annotated assemblies available in public databases, contigs carrying the *epx* genes were aligned using the progressiveMAUVE (1) plugin in Geneious Prime 2021.2.2. The alignments of locally collinear blocks were further enriched using image editing software for clarity and complementary information. For regions upstream and downstream of the *epx* genes, bacterial promoters and transcriptional terminators were predicted *in silico* using BPROM and ARNold (Naville et al., 2011). *In silico* analysis predicted that, in most cases, the toxin gene would be individually transcribed. A notable exception was epx1, which was predicted to be a part of a three-gene operon including two upstream genes coding for a protein of unknown function and a putative phospholipase with ~50% amino acid identity to homologous proteins found in *Clostridium botulinum* and *Chlamydia trachomatis*. Efs, *E. faecalis*; Efm, *E. faecium*; Ehi, *E. hirae*; RM, restriction-modification; TA, toxin-antitoxin; fam., family; TCS, two component system; deH, dehydrogenase.

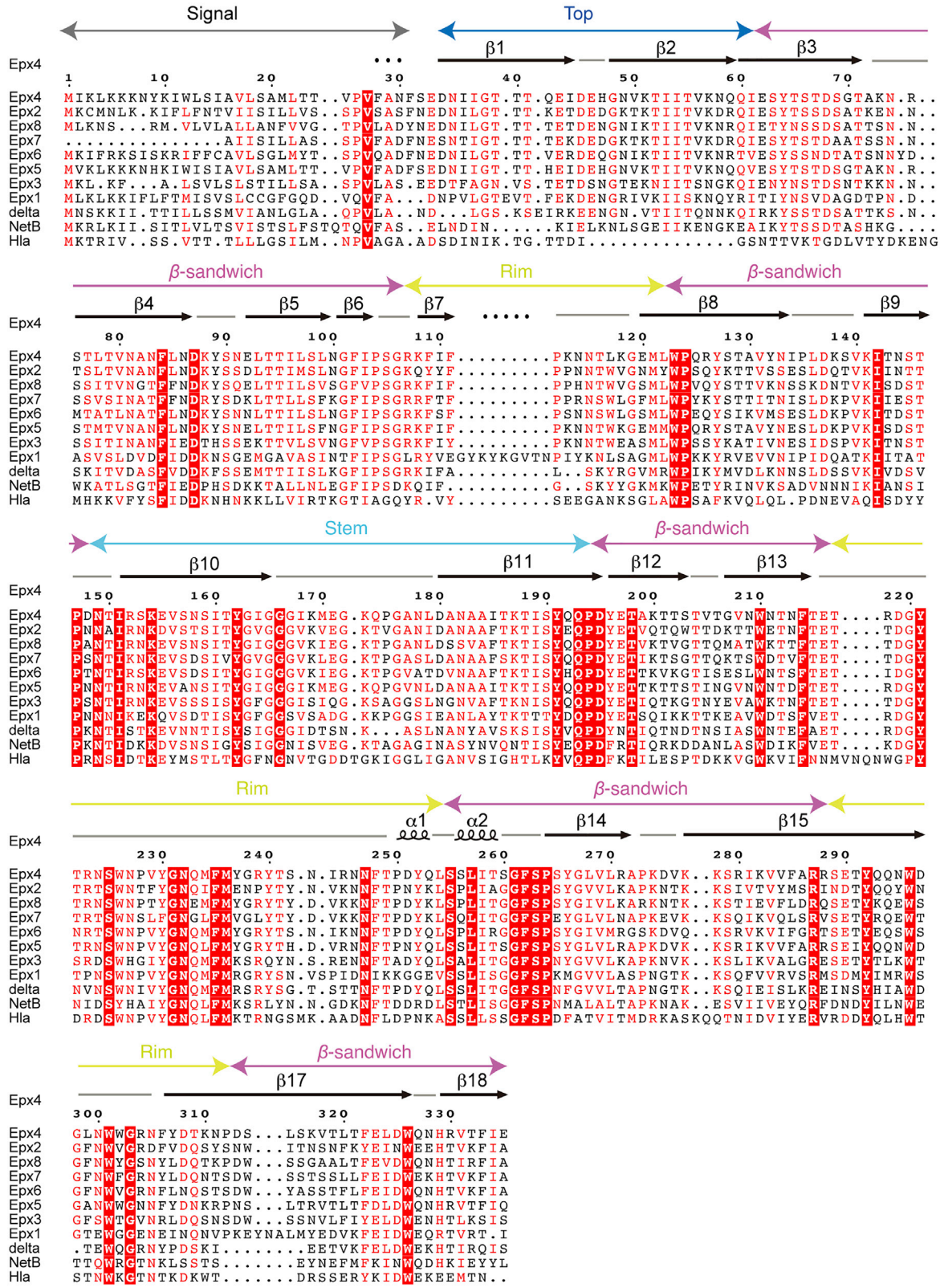

(legend on next page)

Figure S2. Sequence alignment of Epxs and Hla family toxins, related to Figure 1

Structure-based sequence alignment of Epxs and delta toxin (Uniprot No.: B8QGZ7), Hla (Uniprot No.: P09616), and NetB (Uniprot No.: A8ULG6). Residue numbers are shown as dots every ten residues above the alignment. Conserved residues are colored in red; identical residues are shaded red. β labels indicate the β-strands. The alignment was done using ESPript server (https://espript.ibcp.fr/ESPript/ESPript)

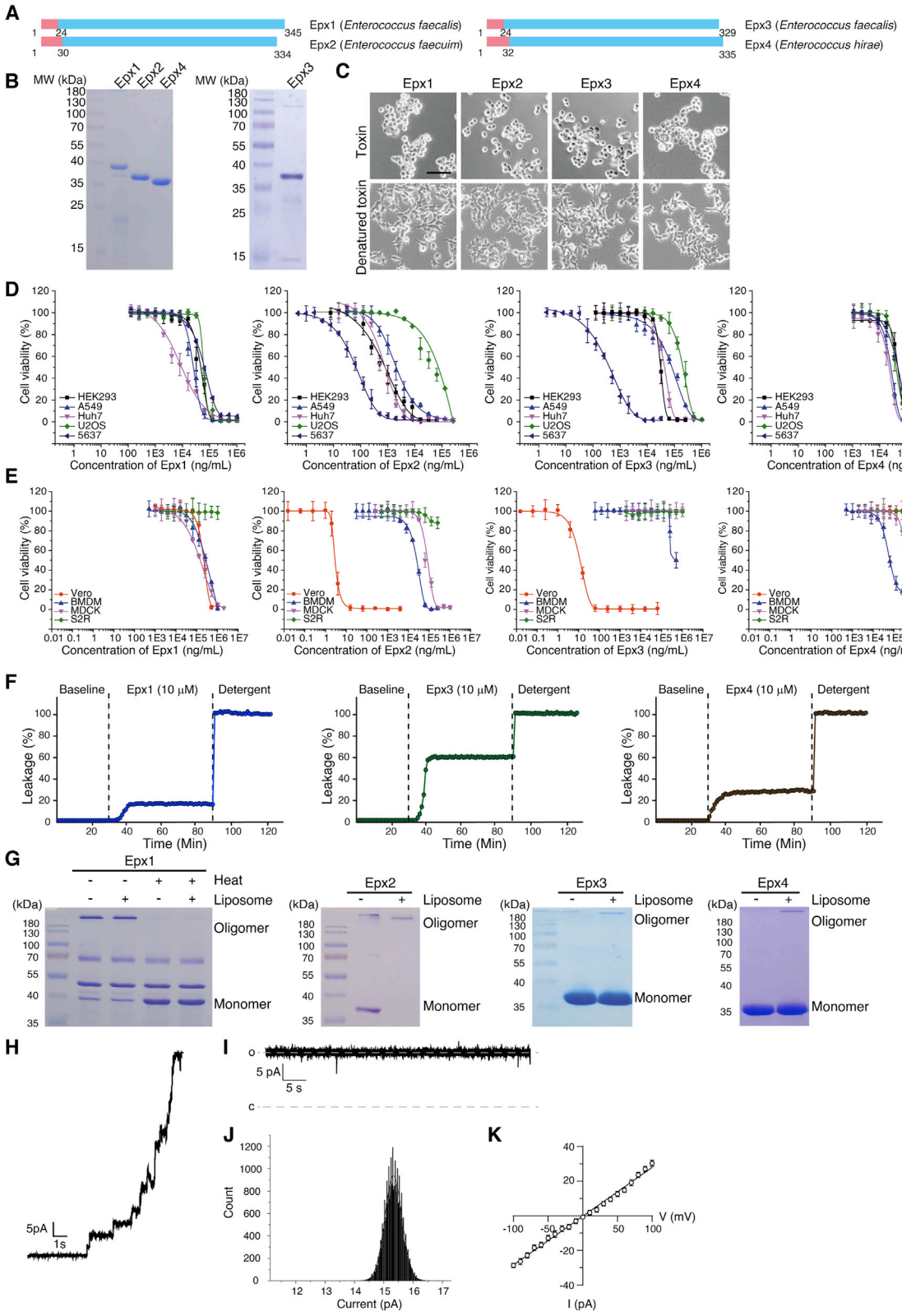

(legend on next page)

Figure S3. Epxs are cytotoxic to mammalian cells and Epxs form oligomeric pores on liposomes, related to Figure 1 and Figure 3

(A) Schematic diagram of Epx1, 2, 3, and 4 proteins. The numbers indicate the position of amino acid residues. The N-terminal signal sequences are predicted using SMART server (http://smart.embl-heidelberg.de).

(B) Recombinant Epx1, 2, 3, and 4 proteins without signal sequences were expressed and purified from *E. coli* and are shown on SDS-PAGE gels with Coomassie blue staining.

(C) Recombinantly produced Epx1, 2, 3, and 4 proteins (100 μg/mL, 10 min incubation) induced morphological changes in HEK293 cells, while heat-denatured proteins showed no toxicity. Scale bar: 50 μm.

(D) A panel of human cell lines (HEK293, A549, Huh7, U2OS, and 5637) were exposed to serial two-fold dilutions of Epx1, Epx2, Epx3, or Epx4 for 4 h. Cell viability was measured using MTT assays and plotted over toxin concentrations. Error bars indicate mean ± SD, N = 3.

(E) Vero cells from African green monkey, immortalized bone marrow-derived macrophage (BMDM) cells from mice, MDCK cells from dogs, and S2R+ cells from *Drosophila* were exposed to serial dilutions of Epx1, Epx2, Epx3, or Epx4 for 4 h. Cell viability was measured using MTT assays and plotted over toxin concentrations. Error bars indicate mean ± SD, N = 3.

(F) Epx1, Epx3, and Epx4 (10 μM) induce leakage of liposomes and release of fluorescent dye Sulforhodamine B. The amounts of leakage were plotted as percentages of the total amount of Sulforhodamine B released by the detergent Triton X-100 (4% v/v).

(G) Epxs with or without incubation with liposomes (1 h) were analyzed on 4%-20% SDS-PAGE and by Coomassie blue staining. Epx1 forms high molecular-weight SDS-resistant oligomers even without incubation with liposomes, which was abolished after heating. Epx2, Epx3, and Epx4 form high molecular-weight SDS-resistant oligomers after incubation with liposomes.

(H–K) Electrical properties of the Epx1 pore on planar lipid bilayers. Under +20 mV holding potential, addition of Epx1 at 100 μg/mL into the planar lipid bilayers resulted in multiple pores (H). Representative trace of Epx1 pores at +50 mV potential is shown in (I). Current histogram of Epx1 pore is shown in (J). The data were fitted by a single Gaussian distribution to determine the mean current (black trace). I/V plot of the Epx1 pore is shown in (K).

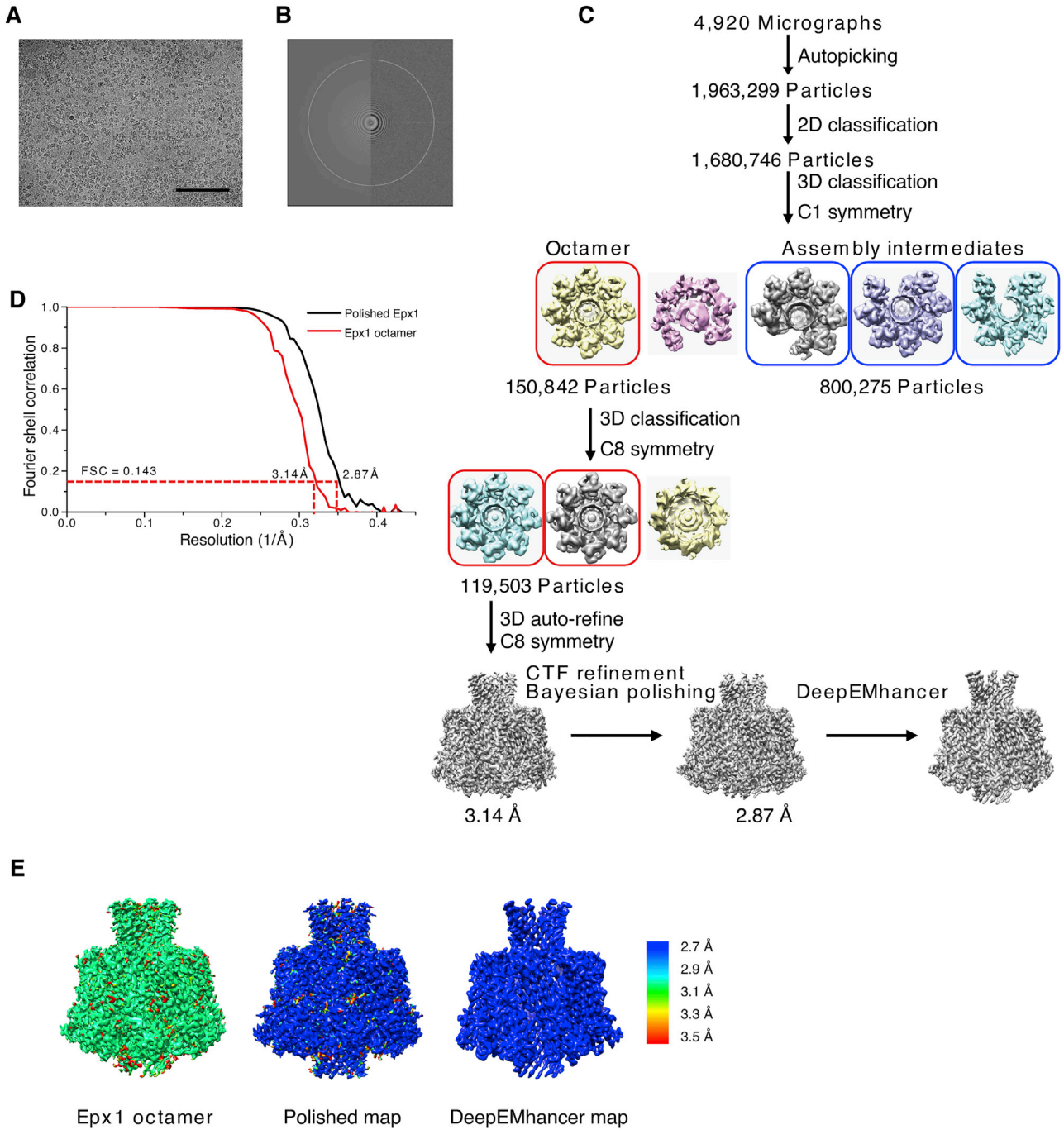

Figure S4. Cryo-EM data collection and processing, related to Figure 3

(A) Representative Cryo-EM micrograph of Epx1. Scale bar = 100 nm.

(B) The corresponding Fourier transformation of (A).

(C) 1,963,299 particles were picked from 4,920 micrographs. Through 2D classification and two rounds of 3D classification, 119,503 octamer particles were selected for the final reconstruction.

(D) Gold-standard FSC curve based on the FSC = 0.143 criterion.

(E) Local resolution maps of Epx1 oligomers are shown as a spectrum ranging from blue (2.7 Å) to red (3.5 Å).

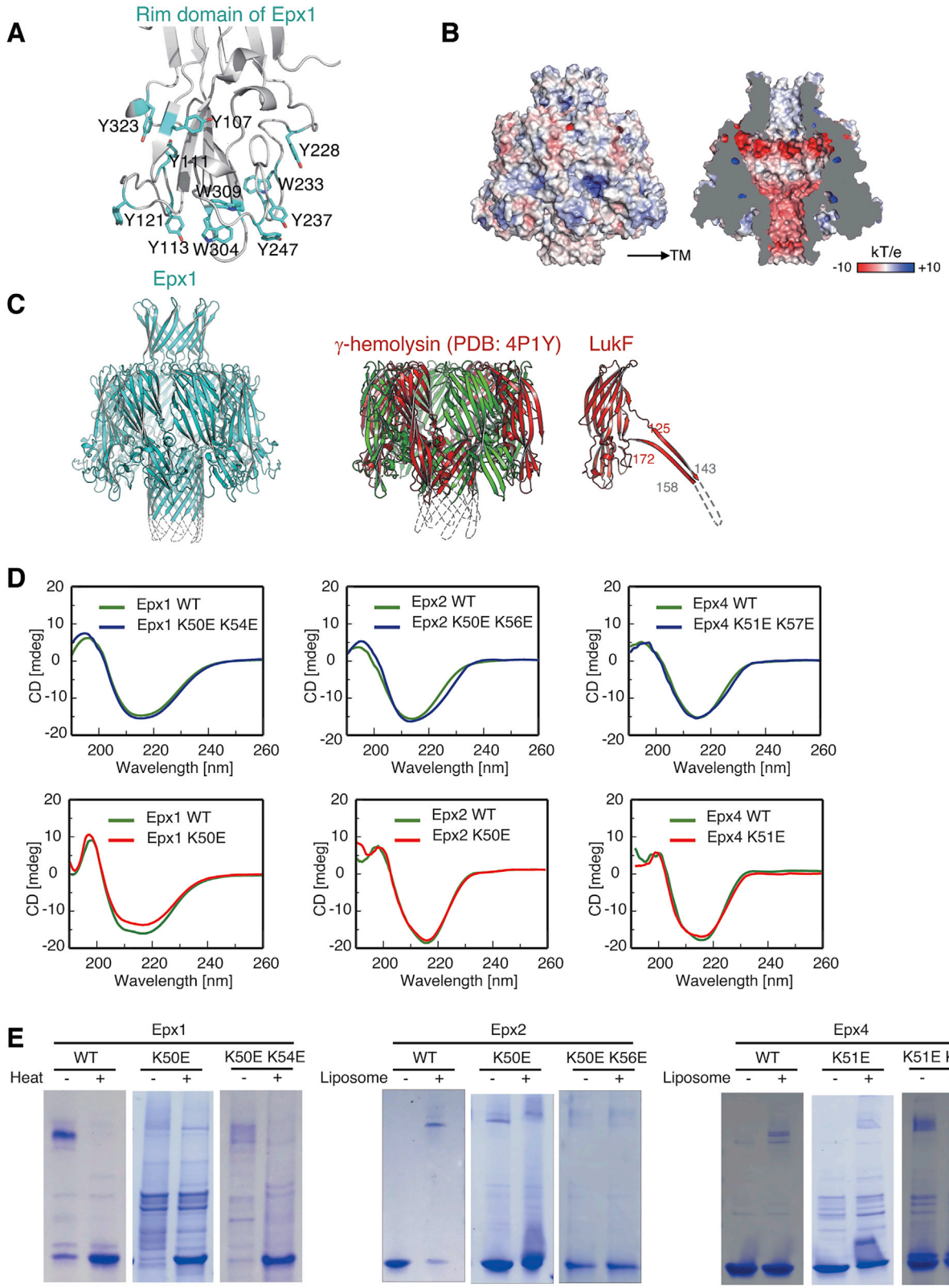

(legend on next page)

Figure S5. Structural characterization of Epx1 and the top domain, related to Figure 3

(A) Cartoon representation of the rim domain of Epx1. The side chains of exposed aromatic residues are shown in stick representation and labeled.

(B) Electrostatic surface views of the Epx1 pore viewed from the external surface (left panel) or as an internal slide (right panel). Electrostatic potential is expressed as a spectrum ranging from −10 kT/e (red) to +10 kT/e (blue). TM, transmembrane.

(C) Comparison of Epx1 oligomers with the reported prepore structure of γ-hemolysin (PDB: 4P1Y) (Yamashita et al., 2014). The two components of γ-hemolysin, LukF and Hlg2, are shown as red and green color respectively.

(D) Circular dichroism spectroscopy analysis of Epxs and Epx mutants.

(E) Designed mutations in the top domains of Epx1 (K50E, K50E/K54E), Epx2 (K50E, K50E/K56E), and Epx4 (K51E, K51E/K57E) reduced the efficacy of forming uniform SDS-resistant oligomers, analyzed by 4%-20% SDS-PAGE gels and Coomassie blue staining.

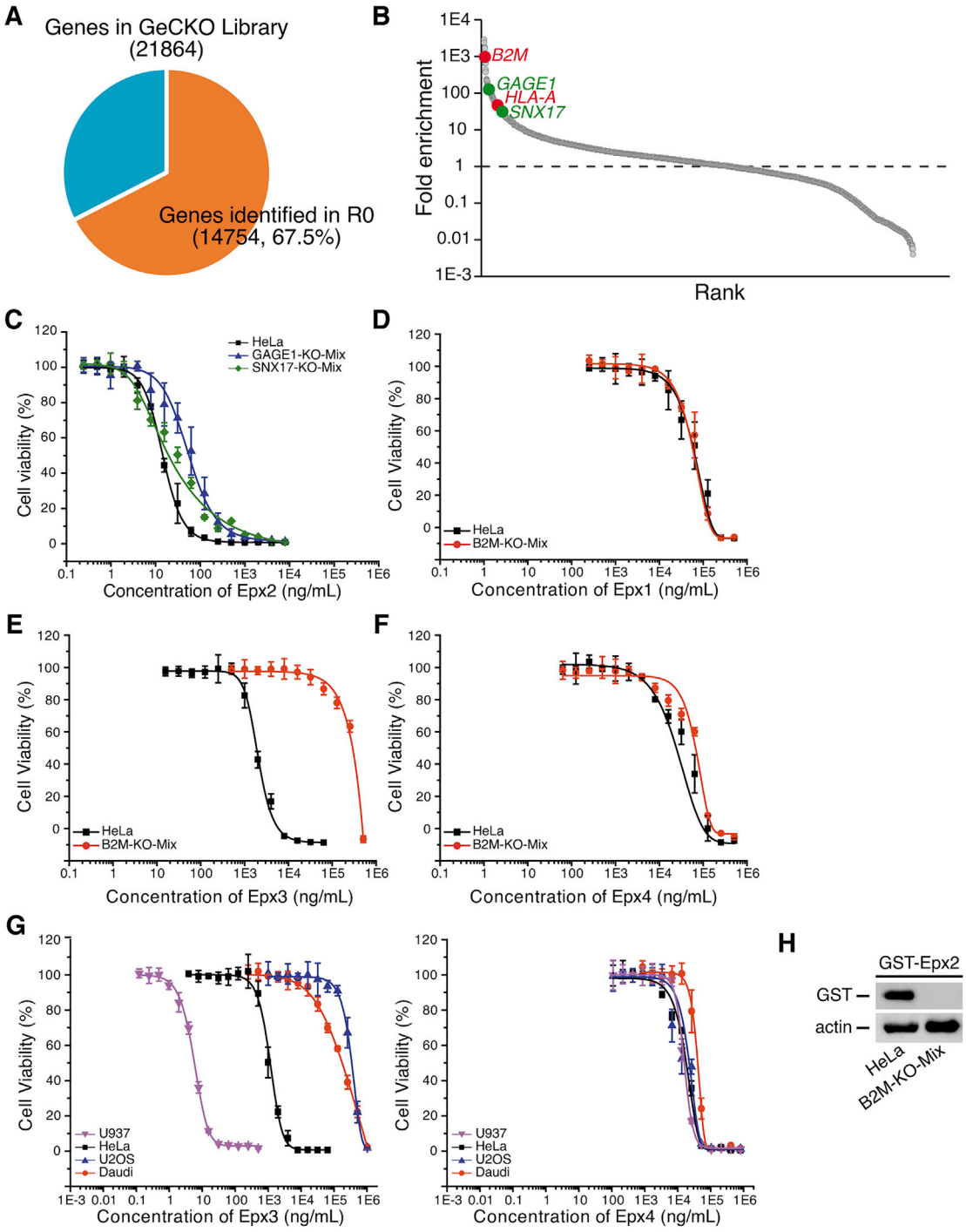

Figure S6. Genome-wide CRISPR-Cas9 screen and validation, related to Figure 4

(A) The recovery rates of genes identified in initial cell library (R0) compared with the original GeCKO-v2 library.

(B) Genes identified in round 2 (R2, the final surviving cells) are plotted based on their fold-enrichment of total sgRNA reads compared with the initial cell library. Selected top hits are marked.

(C) Mixed stable GAGE1 and SNX17 KO HeLa cells were generated using CRISPR-Cas9 approach. These KO cells and the control WT cells were exposed to serial dilutions of Epx2 for 4 h, and cell viability was measured using MTT assays.

(D–F) WT HeLa and B2M KO cells were exposed to serial dilutions of Epx1(D), Epx3 (E), and Epx4 (F) for 4 h. Cell viability was measured using MTT assays.

(G) The sensitivity of U937, HeLa, U2OS, and Daudi cells to Epx3 and Epx 4 were analyzed by MTT assays.

(H) GST-Epx2 were incubated with HeLa and B2M KO cells on ice (50 μg/mL, 40 min). Cell lysates were harvested and analyzed by immunoblot detecting bound GST-Epx2 using an anti-GST antibody. Actin served as a loading control.

(C–G): Error bars indicate mean ± SD, N = 3.

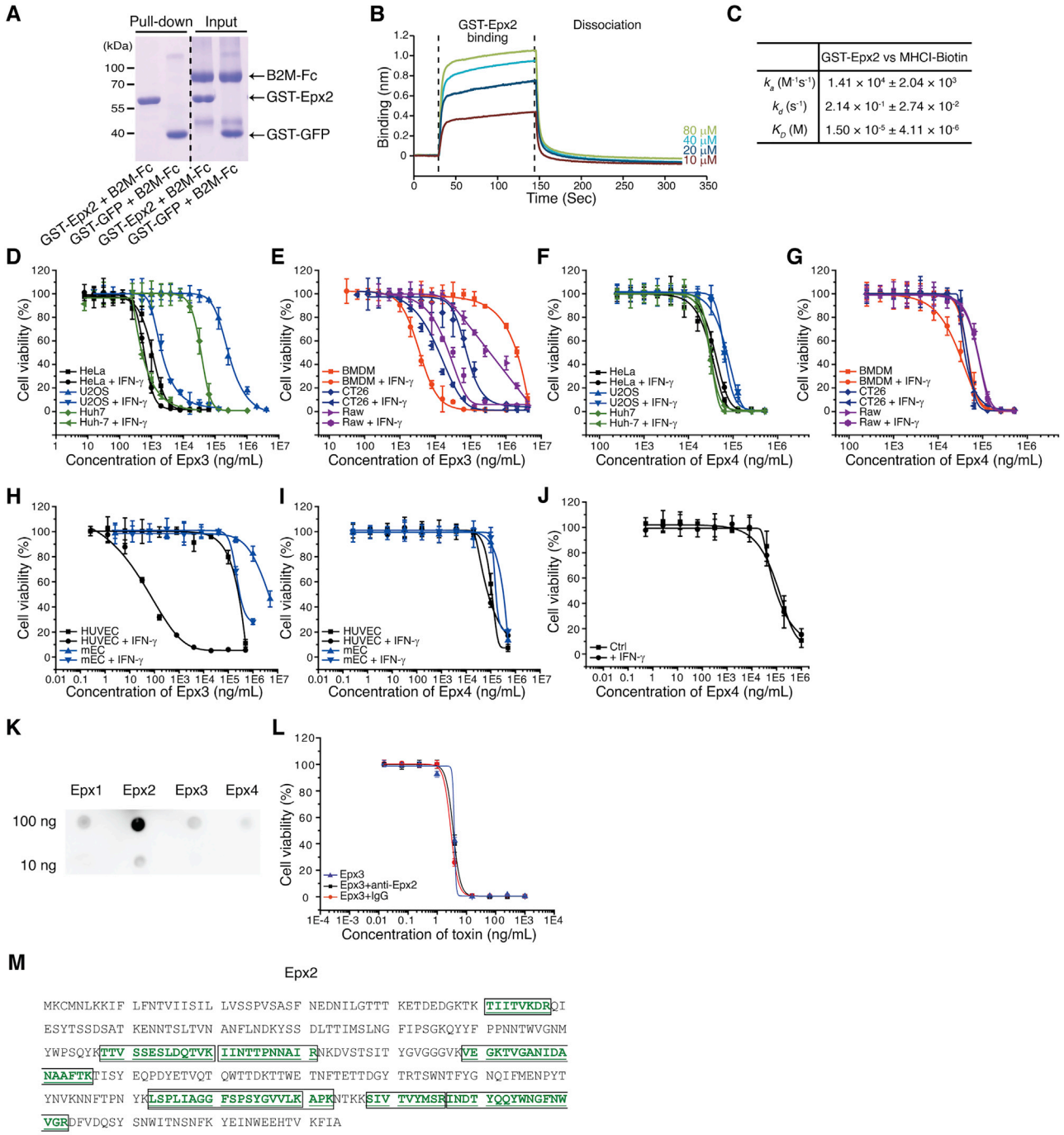

Figure S7. IFN-γ treatment sensitizes cells to Epx3 and characterization of an Epx2 antibody, related to Figures 5–7

(A) GST-Epx2 and recombinantly purified B2M-Fc were mixed and incubated for 2 h. Pull-down assays were carried out using glutathione agarose beads and samples were run on 12% SDS-PAGE gels with Coomassie blue staining.

(B and C) The binding kinetics and affinity between GST-Epx2 and HLA-I complex were determined using biolayer interferometry. Representative sensorgrams of different concentrations of GST-Epx2 are shown in (B) and binding affinities are listed in (C).

(D and E) The sensitivities of three human cell lines (A) and three mouse cell lines (B) to Epx3, with or without IFN-γ treatment, were analyzed by MTT assays.

(F and G) Human (C) and mouse (D) cells are insensitive to Epx4, and sensitivity was not changed by IFN-γ treatment.

(H) HUVEC became highly sensitive to Epx3 after exposure to IFN-γ. IFN-γ treatment also slightly increased the sensitivity of mEC to Epx3.

(I) HUVEC and mEC were not sensitive to Epx4 and IFN-γ treatment did not change their sensitivity to Epx4.

(legend continued on next page)

(J) Human organoids were not insensitive to Epx4 and IFN-γ treatment did not change their sensitivity to Epx4.
(K) Dot-blot analysis showed that the rabbit polyclonal Epx2 antibody recognizes Epx2 but not Epx1, 3, or 4.
(L) Epx2 antibody does not affect the toxicity of Epx3 on HeLa cells.
(M) Culture supernatant of *E. faecium* DIV0147 was subjected to mass spectrometry analysis, which identified eight peptide fragments in Epx2. The protein sequence of Epx2 is shown, with identified eight peptides underlined.
All panels: error bars indicate mean ± SD, N = 3.